ACS APPLIED ENERGY MATERIALS

Article

Rational Management of Photons for Enhanced Photocatalysis in Structurally-Colored Nanoporous Anodic Alumina Photonic Crystals

Siew Yee Lim, Cheryl Suwen Law, Marijana Markovic, Lluis F. Marsal, Nicolas H. Voelcker, Andrew D. Abell, and Abel Santos

ACS Appl. Energy Mater., **Just Accepted Manuscript** • DOI: 10.1021/acsaem.8b01721 • Publication Date (Web): 08 Jan 2019

ACS Publications

is published by the American Chemical Society. 1155 Sixteenth Street N.W., Washington, DC 20036

Rational Management of Photons for Enhanced Photocatalysis in Structurally-Colored Nanoporous Anodic Alumina Photonic Crystals

*Siew Yee Lim[1,2,3], Cheryl Suwen Law[1,2,3], Marijana Markovic[4,5], Lluís F. Marsal[*6], Nicolas H. Voelcker[*7,8,9,10], Andrew D. Abell[*2,3,11] and Abel Santos[*1,2,3]*

[1]School of Chemical Engineering, The University of Adelaide, Adelaide, South Australia 5005, Australia.
[2]Institute for Photonics and Advanced Sensing (IPAS), The University of Adelaide, Adelaide, South Australia 5005, Australia.
[3]ARC Centre of Excellence for Nanoscale BioPhotonics (CNBP), The University of Adelaide, Adelaide, South Australia 5005, Australia.
[4]School of Agriculture Food and Wine, The University of Adelaide, Adelaide, South Australia 5064, Australia.
[5]Center of Chemistry, Institute of Chemistry, Technology and Metallurgy, University of Belgrade, Belgrade, Belgrade 11000, Serbia.
[6]Department of Electronic, Electric, and Automatics Engineering, Universitat Rovira i Virgili, Tarragona, Tarragona 43007, Spain.
[7]Melbourne Centre for Nanofabrication, Victorian Node of the Australian National Fabrication Facility, Monash University, Melbourne, Victoria 3168, Australia.
[8]Monash Institute of Pharmaceutical Sciences, Monash University, Melbourne, Victoria 3052, Australia.
[9]Commonwealth Scientific and Industrial Research Organisation (CSIRO), Melbourne, Victoria 3168, Australia.
[10]INM-Leibniz Institute for New Materials, Campus D2 2, Saarbrücken 66123, Germany.
[11]Department of Chemistry, The University of Adelaide, Adelaide, South Australia 5005, Australia.

*E-mails: lluis.marsal@urv.cat ; nicolas.voelcker@monash.edu ; andrew.abell@adelaide.edu.au ; abel.santos@adelaide.edu.au

KEYWORDS: Photocatalysis, Photonic Crystals, Slow Photons, Stopband, Pulse Anodization.

ABSTRACT: A comprehensive study on the engineering of titanium dioxide-functionalized nanoporous anodic alumina distributed Bragg reflectors (TiO_2-NAA-DBRs) for photocatalysis enhanced by the "slow photon" effect is presented. The photocatalytic performance of these composite photonic crystals (PCs) is assessed by monitoring photodegradation of a variety of organic molecules with absorbance bands across the spectral regions. This study demonstrates that photocatalytic performance of TiO_2-NAA-DBRs is enhanced by the "slow photon" effect when the edges of the PC's photonic stopband (PSB) fall within the absorbance band of the organic molecules. The photocatalytic performance is significantly enhanced when the PSB's red edge is in close proximity to the absorbance band of the organic molecules. Overall photocatalytic degradation is also dependent on the total pore length of the PC structure, charge of the organic molecules, percentage of vis-NIR irradiation and matrix complexity (i.e. interfering ions and molecules) when the PC's PSB is partially or entirely misaligned with respect to the absorbance band of the organic molecules. Finally, the real-life application of TiO_2-NAA-DBRs to degrade pollutants such as pesticides in environmental matrices is

demonstrated. This study provides new insights into the development of rationally engineered, high-performing, safe and reusable photocatalyst systems.

INTRODUCTION

Photonic crystals (PCs) are micro/nanostructures that play important roles in light-driven applications, including photocatalysis[1-5], photovoltaics[6-8], optics and biosensing[9]. The rational design of the PC's structure amplifies light-matter interactions by controlling, modulating, and trapping the propagation of electromagnetic waves across its structure *via* Bragg diffraction, multiple scattering, and the "slow photon" effect.[10-12] Bragg diffraction forbids light from propagating across the PC's structure due to its characteristic photonic stopband (PSB). Multiple scattering reduces light loss due to reflection and increases the optical path length of the flowing light at spectral regions that are away from the PC's PSB. As a result, light is internally trapped within the PC, enhancing its light-confining properties. Furthermore, photons propagate with strongly reduced group velocity ("slow photons") at the frequency edges of the PC's PSB, giving rise to the so-called "slow photon" effect. Slow photons are strongly localized in different dielectric parts of the PC's structure (i.e. sections of high and low refractive index) at the edges of the PC's PSB (i.e. red and blue edges), enabling a longer lifetime of photons at these spectral regions. This leads to an enhancement in the overall optical absorbance of the material. Besides the enhanced light-matter interactions attributed to the PC effect, nanoporous semiconductor PCs provide high specific surface area that increases the number of functional sites available for reactions. The nanoporous structure facilitates mass transport of ionic and molecular species involved in these photo-chemical processes, and light harvesting capabilities for efficient management of photons at high-irradiance spectral regions (i.e. visible and IR).[1,4]

Nanoporous semiconductor PC structures are superior to their nanoparticle-based counterparts in light-driven applications. Particulate systems have a propensity to aggregate[13] and are also difficult to be recovered after use[14-15], becoming potentially toxic to the

environment[16]. Furthermore, most semiconductor nanoparticles only absorb light in the UV region (i.e. ~ 5% of the solar spectrum) due to a high energy bandgap and the rapid recombination of photogenerated charge carriers at their surface[17-20]. These factors limit the capability of nanoparticle-based systems to attain efficient and practical photon-to-electron conversion rates for real-life light-driven processes. Films of nanoporous semiconductor PCs can overcome these limitations due to their robust structure and unique set of physical and chemical properties, which allows rational management of photons at the nanoscale to speed up redox reactions. The advantages of photocatalyst semiconductor PC structures make them desirable for a broad range of applications, including generation of hydrogen energy[21-24], purification of air and water[1-5,25], production of chemicals such as ammonia (NH_3)[26], and carbon dioxide (CO_2) reduction for environmental remediation[27-28]. Nanoporous semiconductor PCs enable control of light-matter (i.e. photons-semiconductor) interactions at the nanoscale in order to generate extra electron/hole (e^-/h^+) pairs and produce strongly oxidizing and non-selective radicals for redox reactions.[29] Pure semiconductor PCs with inverted opal structures have been widely employed for photocatalysis, particularly in water purification.[1,30-32] These semiconductor PC structures show enhanced performances in the photodegradation of organic dye molecules under visible light irradiation when compared to nanoparticle and non-porous film counterparts.

Photocatalytic enhancement in these systems is associated with the overall PC effect, particularly with the "slow photon" effect when the edges of the PC's PSB are tuned with respect to the absorbance band of the organic dye or to the electronic bandgap of the material. However, Zheng *et al*.[1] and Meng *et al*.[30] demonstrated that the performance of inverted opal PC structures to degrade organic molecules can be inhibited when the absorbance band of these molecules is located in the UV spectral region. These studies indicate that the photocatalytic capability of these PC structures is limited to organic molecules with absorbance bands within

the visible spectral region under visible light irradiation. Furthermore, inverted opal PCs have other intrinsic limitations, including limited versatility in tuning the PSB across the spectral regions, restriction to 3D nanostructures, formation of structural defects (i.e. scattering centers), limited to small domain areas, and require a long synthesis process (>24 h).[4,33-36] Significant effort has been devoted to developing alternative nanoporous semiconductor PC structures capable of addressing these limitations to achieve enhanced performances for photocatalysis. Amongst these, nanoporous PCs produced by electrochemical anodization of valve metals have shown promising results in photocatalysis, including titanium dioxide nanotubes[37-40] and nanoporous anodic alumina (NAA)[4]. Anodization is an industrially scalable, eco-friendly, highly-controllable, and low-cost electrochemical process broadly used in metal finishing industry to modify the properties of metals such as color, brightness, wettability, and corrosion protection. The generation of nanoporous PCs by anodization is a versatile approach that enables the development of PC systems with precisely engineered optical properties for different applications, including optical sensing and biosensing[41-44], light filtering[45-46], energy harvesting[6-8], and photocatalysis[4,37-40]. NAA produced by anodization of aluminum is an excellent platform material to develop PC structures due to its highly versatile and controllable nanoporous structure. However, NAA has a wide energy bandgap (i.e. 7.0–9.5 eV) that prevents the direct use of NAA-PCs in photocatalysis. Despite this intrinsic limitation, we have recently demonstrated that the chemical modification of NAA-PCs with layers of semiconductor materials with narrower energy bandgap such as titanium dioxide (TiO_2 – 3.20–3.35 eV) does enable the production of high-performing composite photocatalysts that outperform conventional photocatalyst platforms.[4] NAA-PCs have distinctive PSBs, the features of which can be readily tuned across the spectral regions by engineering the effective medium of NAA in a multi-dimensional fashion, through various anodization approaches.[45,47-52] These NAA-PC platforms include optical microcavities[47,48], distributed Bragg reflectors

(DBR)[45,49], linear variable bandpass filters[50], gradient-index filters[51], and hybrid PCs[52]. These PC structures provide new opportunities to rationally utilize the "slow photon" effect to attain an efficient management of photons at the nanoscale for photocatalytic applications.

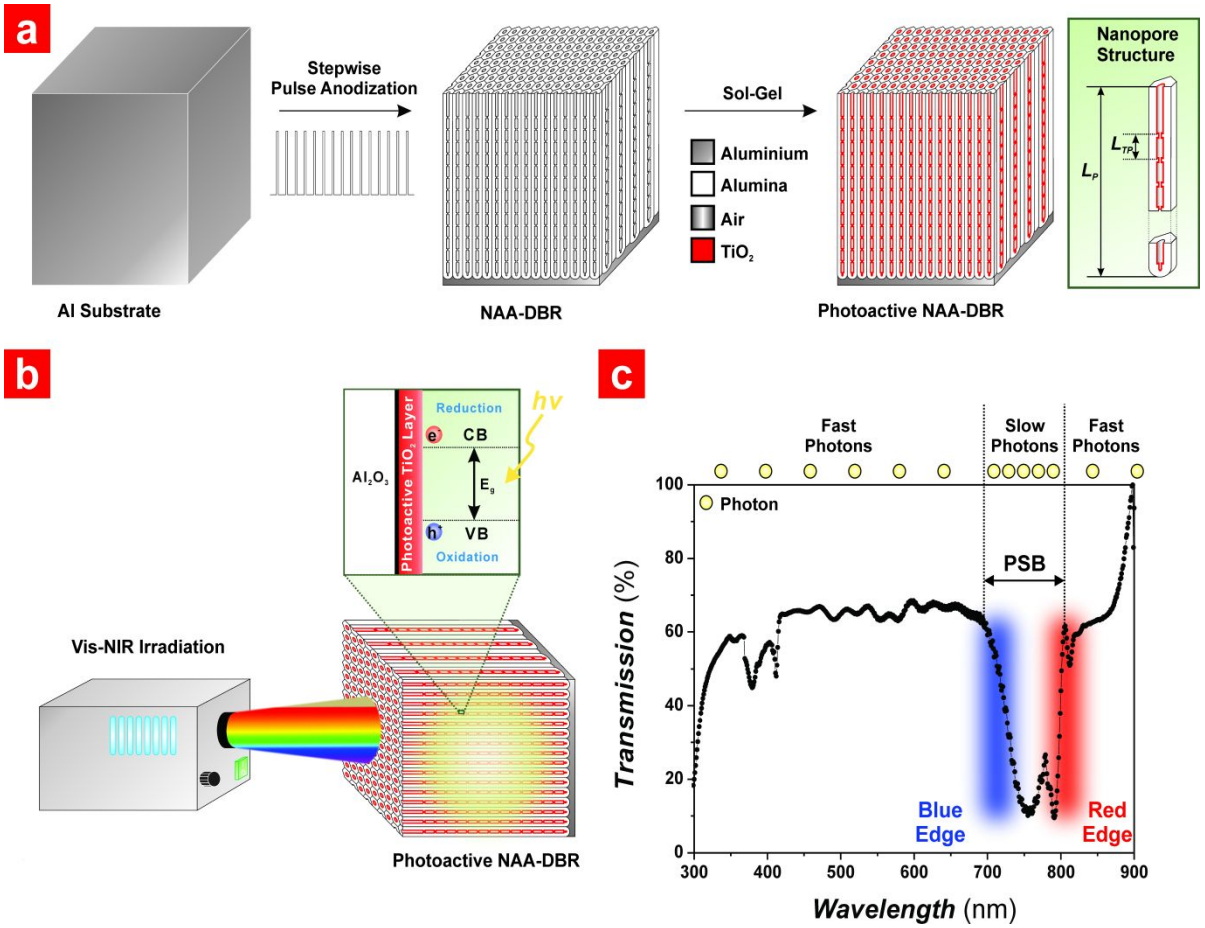

Figure 1. Fabrication and photocatalytic assessment of titania-functionalized structurally-colored nanoporous anodic alumina distributed Bragg reflectors (TiO_2-NAA-DBRs). a) Schematic illustrating the combination of stepwise pulse anodization (STPA) and sol-gel functionalization method used to fabricate TiO_2-NAA-DBRs with a visual description of the nanoporous structure of these photonic crystals (i.e. pore length – L_P and period length – L_{TP}). b) Schematic design of the photocatalytic assessment of TiO_2-NAA-DBRs under simulated visible-NIR irradiation conditions with details showing the chemical and electronic band structures of the composite photonic structures (note: E_g = energy band gap, hv = excitation energy, CB = conduction, and VB = valence band). c) Representative transmission spectrum of a reference NAA-DBRs showing the effect of the photonic stopband (PSB) and its blue and red edges on the group velocity of photons across the spectral regions (note: NAA-DBR produced with anodization period – T_P = 1400 s, number of anodization pulses – N_P = 150 pulses, and pore widening time – t_{pw} = 0 min, where the medium filling the nanopores is water).

Herein, we develop and study photoactive TiO_2-functionalized structurally-colored NAA-DBRs as photoactive PC platforms for enhanced photocatalytic degradation of organic molecules. NAA-DBRs are fabricated by stepwise pulse anodization (STPA) and subsequently functionalized with photoactive layers of TiO_2 by sol-gel method (**Figure 1**). Photocatalytic

performance of TiO_2-NAA-DBRs is assessed under controlled visible-NIR irradiation conditions by a systematic modification of several parameters, including the anodization period (i.e. features of PSB), concentration of hydrogen peroxide, characteristics of model organic molecules, and complexity of liquid matrix. This approach enables the identification of photocatalytic enhancements by the "slow photon" effect, using TiO_2-NAA-DBRs as model photocatalyst platforms under controlled irradiation conditions. Furthermore, other critical factors for real-life applications such as reusability and photodegradation of model pesticides by TiO_2-NAA-DBRs are demonstrated.

EXPERIMENTAL SECTION

2.1. Materials. High purity (99.9997%) aluminum (Al) foils 0.32 mm thick were purchased from Goodfellow Cambridge Ltd. (UK). Hydrochloric acid (HCl), copper (II) chloride ($CuCl_2$), perchloric acid ($HClO_4$), sodium chloride (NaCl), titanium (IV) butoxide ($Ti(OBu)_4$), hydrogen peroxide (H_2O_2), methyl orange (MO), methylene blue (MB), rhodamine B (RhoB), and 4-chlorophenol (4-CP) were supplied by Sigma-Aldrich (Australia). Ethanol (EtOH – C_2H_5OH) and sulfuric acid (H_2SO_4) were purchased from ChemSupply (Australia). Ultrapure Milli-Q® water (18.2 MΩ cm) was used in the preparation of all the aqueous solutions used in this study.

2.2. Fabrication of NAA-DBRs. NAA-DBRs were produced by stepwise pulse anodization (STPA) under current density control conditions.[49] Prior to anodization, 1.5 x 1.5 cm^2 square chips were sonicated in ethanol and water for 15 min each, dried under air stream and electropolished in a mixture of EtOH and $HClO_4$ 4:1 (*v*:*v*) at 20 V and 5 ºC for 3 min. The electropolished Al chips were anodized in an aqueous solution of 1.1 M H_2SO_4 with 25 *v*% of EtOH at 1 ºC. The anodization process started with a constant current density of 1.120 mA cm^{-2} for 1 h to achieve a homogeneous pore growth rate prior to stepwise pulse anodization. The anodization profile was subsequently switched to stepwise pulse mode, where the current density was pulsed between high (J_{max} = 1.120 mA cm^{-2}) and low (J_{min} = 0.280 mA cm^{-2}) current

density values following a stepwise modulation for a total of 150 anodization pulses (N_P). The anodization period (T_P) (i.e. time between consecutive pulses) was modified from 900 to 1600 s with an interval (ΔT_P) of 100 s. Note that T_P is given by **Equation 1**:

$$T_P = t_{max} + t_{min} \quad (1)$$

where t_{max} and t_{min} are the time for maximum and minimum current density pulses (i.e. J_{max} = 1.120 mA cm^{-2} and J_{min} = 0.280 mA cm^{-2}), respectively, and the time ratio for t_{max} and t_{min} (t_{max}:t_{min}) was set to 1:4 for T_P = 900 to 1600 s.

2.3. Surface Functionalization of NAA-DBRs with Photoactive Layers of TiO_2. The inner surface of NAA-DBRs was chemically functionalized with TiO_2 photoactive layers through the sol-gel method. The TiO_2 sol was prepared by magnetically stirring a mixture of titanium (IV) butoxide (3 *v*%) and EtOH (97 *v*%) for 10 min. NAA-DBRs were subsequently soaked in the TiO_2 sol for 24 h. The surface-functionalized NAA-DBRs were washed with EtOH to remove any excess of TiO_2 sol and titanium (IV) butoxide. The TiO_2-NAA-DBRs were then dried in an oven at 50 ºC for 10 min to evaporate any remaining EtOH residues.

2.4. Optical Characterization. Prior to transmission spectra acquisition, NAA-DBRs were chemically etched in a saturated solution of HCl/$CuCl_2$ using a 5 mm diameter circular window etching mask to selectively dissolve the underlying Al substrate at the backside. Transmission spectra of chemically etched NAA-DBRs fabricated with different anodization periods were obtained in air and water from 200 to 800 nm at normal incidence (i.e. θ = 0^o), using a UV-visible spectrophotometer (Cary 300, Agilent, USA). The absorbance spectra of 5 mg L^{-1} organics (i.e. MO, RhoB, MB, and 4-CP) in a quartz cuvette of 10 mm path length were acquired from 200 to 800 nm to determine the absorbance bands of the organics. The interferometric color of NAA-DBRs in air and water was characterized by digital pictures,

using a Canon EOS 700D digital camera equipped with a Tamron 90 mm F2.8 VC USD macro mount lens with autofocus function under natural light illumination.

2.5. Photocatalytic Degradation of Organics under Controlled Irradiation Conditions. Photocatalytic performance of TiO_2-NAA-DBRs fabricated with various T_P was assessed under simulated solar light irradiation conditions, using the degradation of a model organic dye, methylene blue (MB), with well-defined absorbance band within the visible spectral range (i.e. MB – $\lambda_{Abs\text{-}MB}$ = 664 nm) as an efficiency indicator. A 2 mL mixture of 5 mg L^{-1} of MB and 100 mM H_2O_2 solution was pipetted into a transparent cuvette. The TiO_2-NAA-DBRs, which had an effective area of 1 cm^2, were then submerged inside the organic mixture. The solution was magnetically stirred in a dark vessel (i.e. solar simulator) for 30 min to achieve the adsorption-desorption equilibrium prior to irradiation. The system was subsequently illuminated with simulated solar light irradiation using a 150 W (~3000 lumen) halogen lamp (HL250-A, Amscope, Australia) at room temperature. To determine the concentration of MB at specific time intervals, the absorbance of the MB solution at $\lambda_{Abs\text{-}MB}$ = 664 nm for each illumination time interval (i.e. 15 min) was analyzed by UV-visible spectroscopy. The relationship between the absorbance intensity and the concentration of MB was established by a calibration line to obtain the photocatalytic conversion ratio (C_t/C_o), where C_o is the concentration of organic after stirring in the dark for 30 min and C_t is the concentration at illumination time t (**Figure S1 – Supporting Information**). This parameter was used in determining the kinetic model for this photocatalytic system. The effect of the type of organic dye and the concentration of H_2O_2 on the photocatalytic performance of TiO_2-NAA-DBRs fabricated with T_P = 1200 s was systematically assessed by modifying the organic molecule model (i.e. MB, MO, and RhoB; MO – $\lambda_{Abs\text{-}MO}$ = 464 nm and RhoB – $\lambda_{Abs\text{-}RhoB}$ = 554 nm) and the concentration of H_2O_2 solution (i.e. 12.5, 50.0, 100, and 200 mM), respectively. The reusability of TiO_2-NAA-DBRs fabricated with T_P = 1200 s was assessed under simulated solar light irradiation by repeating

the photocatalytic degradation of MB molecules five times using the same photocatalyst platform. The TiO_2-NAA-DBR was washed in EtOH and water under sonication for 15 min each and dried under air stream before each photocatalytic cycle. To demonstrate the photocatalytic capability of TiO_2-NAA-DBRs for real-life applications, the photodegradation of 4-CP (i.e. $\lambda_{Abs\text{-}4\text{-}CP}$ = 225 nm), a model pesticide, by TiO_2-NAA-DBRs was investigated. Two main parameters were assessed: i) the effect of the anodization period (i.e. T_P = 900, 1200, and 1600 s) and ii) the composition of the aqueous matrix of 4-CP (i.e. milli-Q water, tap water, filtered Torrens river water, and 10 g L^{-1} NaCl aqueous solution).

2.6. Chemical and Structural Characterization. The structural features of NAA-DBRs were characterized using a field emission gun scanning electron microscope (FEG-SEM FEI Quanta 450). FEG-SEM images were analyzed by ImageJ.[54] The chemical composition of NAA-DBRs before and after surface functionalization with TiO_2 was analyzed by energy dispersive X-ray (EDX) spectroscopy during FEG-SEM characterization.

RESULTS AND DISCUSSION

3.1. Fabrication and Structural Characterization of NAA-DBRs. Figure 2 shows a representative STPA profile with a graphical description of the different anodization parameters and a set of representative FEG-SEM images of NAA-DBRs produced by STPA process. The anodization profile reveals that the anodization voltage (i.e. output) follows closely the anodization current density (i.e. input) applied during the STPA process. Thus, the anodization conditions used in our study enable the efficient translation of the anodization current density profiles into changes in the porosity of NAA in depth (**Figure 2a**). The anodization process begins with a constant current anodization step (CA) (**Figure 2b**), which produces a layer of NAA with straight nanopores. This process is followed by the STPA stage, during which stacked layers of NAA with stepwise porosity are generated, as depicted in the FEG-SEM image shown in **Figure 2c**. A top view FEG-SEM image reveals that the nanopores

are evenly and randomly distributed across the surface of NAA-DBRs, with an average nanopore diameter (d_p) measured to be 10 ± 3 nm (**Figure 2d**).

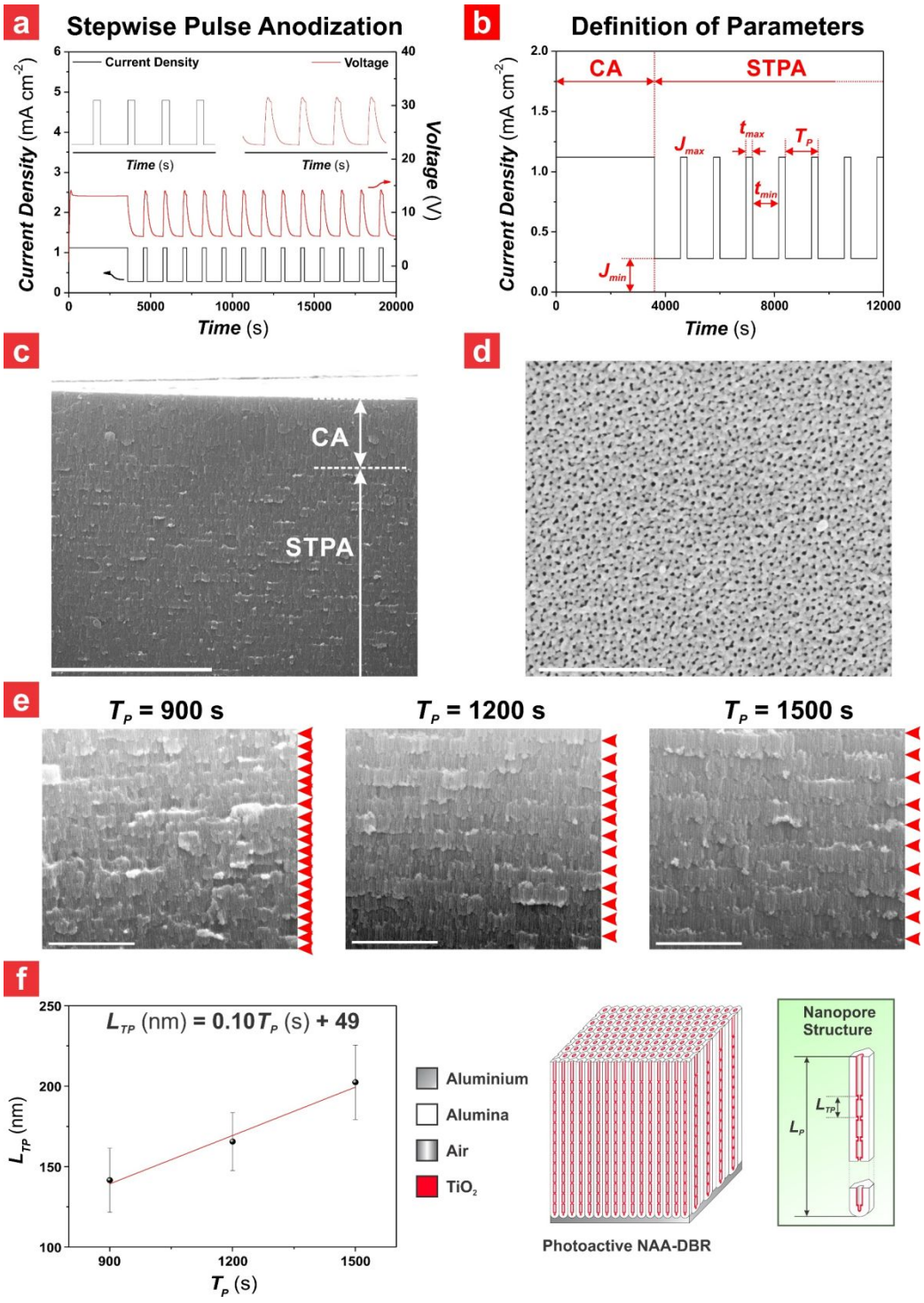

Figure 2. Fabrication and structural characterization of the nanoporous structure of NAA-DBRs fabricated by stepwise pulse anodization (STPA). a) Representative anodization profile used to produce NAA-DBRs with and anodization period (T_P) of 1200 s and 150 anodization pulses (N_P) by STPA approach. b) Graphical definition of the anodization parameters (i.e. J_{min}, J_{max}, t_{min}, t_{max}, and T_P) used to generate the STPA profiles (note: CA = constant current anodization step). c) General cross-sectional FEG-SEM image view of a NAA-DBR (scale bar = 4 µm).

d) Top view FEG-SEM image of a NAA-DBR fabricated with T_P = 900 s and N_P = 150 pulses (scale bar = 500 nm). e) FEG-SEM images showing cross-sectional views of NAA-DBRs fabricated with T_P = 900 s (left), T_P = 1200 s (center) and T_P = 1500 s (right) (scale bar = 1 μm) (note: red arrowheads denote the interfaces between anodization periods, L_{TP}). f) Linear correlation between L_{TP} and T_P (left) with schematic description of L_{TP} in the nanoporous photonic crystal structure (right) (note: error bars denote standard deviation from average measurements obtained from n = 3 independent NAA-DBRs).

A visual analysis of NAA-DBRs fabricated with different anodization period (i.e. T_P = 900, 1200, and 1600 s) demonstrates that the period length (L_{TP}) of the stacked layers of NAA (graphic illustration in **Figure 1a**), as indicated by the red arrowheads shown in the cross-sectional FEG-SEM images shown in **Figure 2e**, increases with T_P. The correlation between L_{TP} and T_P follows a linear relationship, where L_{TP} increases at a rate of 0.10 nm s^{-1} with increasing T_P (**Figure 2f**).

3.2. Effect of Anodization Period and Surface Functionalization on the Optical Properties of NAA-DBRs. Figure 3 depicts the dependence of the optical properties of NAA-DBRs on the anodization period (T_P) in air and water as well as the chemical composition analysis of the NAA-DBRs before and after surface functionalization with photoactive layers of TiO_2. The combined effect of T_P and media filling the nanoporous network of NAA-DBRs on the position of the characteristic photonic stopband (PSB) were systematically studied by modifying T_P from 900 to 1600 s with ΔT_P = 100 s in air and water (H_2O) (**Figure 3a**). It is noteworthy that the photocatalytic reactions assessed in our study were performed in aqueous media. Therefore, establishing the photonic characteristics of NAA-DBRs in water is critical to understand the system's performance and identify photocatalytic performance enhancements associated with the "slow photon" effect. An analysis of the correlation between T_P and the central wavelength (λ_C) of the characteristic PSB establishes a linear relationship between these two parameters in both air and H_2O, with slopes 0.34 ± 0.03 and 0.44 ± 0.04 nm s^{-1}, respectively. In air, the position of the PSB can be tuned from 492 ± 1 to 740 ± 1 nm on varying T_P from 900 to 1600 s. This demonstrates that the position of characteristic PSB red shifts with T_P. This result is further supported by the interferometric color displayed by these NAA-PCs, as indicated by

the digital images shown in **Figure 3a**, and the transmission spectra of NAA-DBRs shown in **Figure S2 (Supporting Information)**. Structurally-colored NAA-DBRs display vivid colors in air, varying from purple (T_P = 900 s), periwinkle (T_P = 1000 s), blue (T_P = 1100 s), green (T_P = 1200 s), yellow (T_P = 1300 s), chartreuse (T_P = 1400 s), orange (T_P = 1500 s) to light brown (T_P = 1600 s). This phenomenon is attributable to a more efficient reflection of light by the PC structure at those spectral regions where the PSB is located.[49] Similarly, the position of the characteristic PSB also red-shifts from 521 ± 1 to 839 ± 2 nm with T_P from 900 to 1600 s when the nanopores of NAA-DBRs are infiltrated with H_2O. The position of the characteristic PSB is red-shifted at an average rate of 65 ± 26 nm s^{-1} on changing the media within the nanoporous network of NAA-DBRs from air to H_2O. This red-shift is due to the infiltration of nanopores with a medium of higher refractive index than that of air (i.e. n_{air} = 1.00 RIU and n_{H2O} = 1.33 RIU).

Figure 3b compiles a set of digital pictures of NAA-DBRs partially covered with transparent tape displaying interferometric colors as a function of T_P and the media infiltrating the nanopores (i.e. air and water). The left part of the photo in each digital image corresponds to the interferometric color displayed by NAA-DBRs in air while the right part corresponds to that in H_2O. As commented above, NAA-DBRs display vivid interferometric colors in air (i.e. purple – T_P = 900 s, periwinkle – T_P = 1000 s, blue – T_P = 1100 s, green – T_P = 1200 s, yellow – T_P = 1300 s, chartreuse – T_P = 1400 s, orange – T_P = 1500 s, and light brown – T_P = 1600 s), which red-shift with T_P. Similarly, the interferometric color also red-shifts with T_P when the nanopores of NAA-DBRs are filled with H_2O. Furthermore, these images indicate that, when the nanopores are filled with H_2O, the interferometric color is also red-shifted for all T_P, except for T_P = 1600 s, which displays light brown interferometric color at both parts of the digital picture. Note that the interferometric color relies upon the position of the characteristic PSB within UV-visible-NIR spectrum. As such, NAA-DBRs featuring the characteristic PSB within

the visible spectrum display interferometric color, from purple to orange, while those NAA-DBRs with PSB in the NIR spectral range are light brown, which is the characteristic color of NAA produced under the fabrication conditions used in this study.

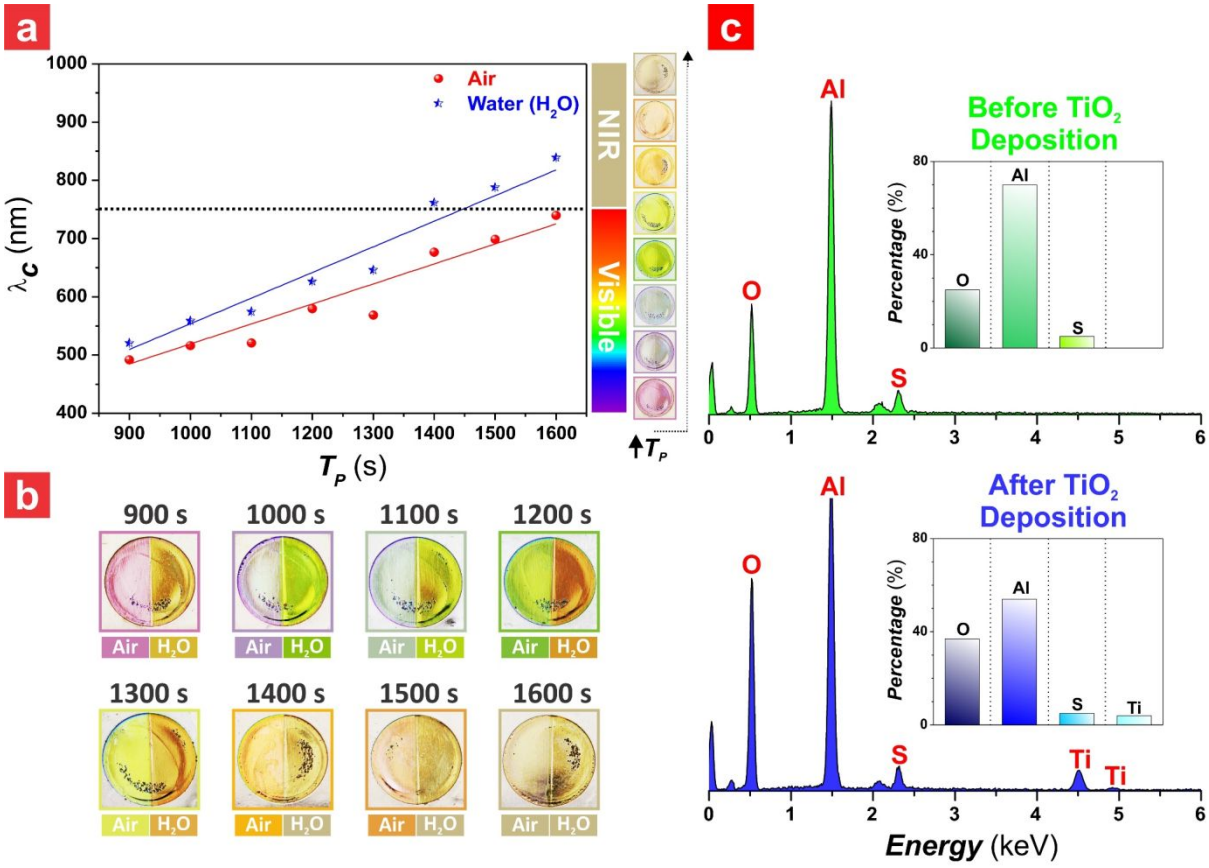

Figure 3. Optical tunability of the PSB of NAA-DBRs by varying anodization period (T_P) and chemical analysis of the composite photonic structures after surface functionalization with photoactive layers of TiO_2. a) Position of the characteristic photonic stopband (PSB - λ_C) as a function of media (left) and digital images displaying the interferometric color of NAA-DBRs from T_P = 900 to 1600 s with ΔT_P = 100 s in air (right) (note: error bars correspond to standard deviation from n = 3 independent measurements). b) Interferometric color of NAA-DBRs as a function of T_P and media (note: sample diameter 1 cm). c) Energy dispersive X-ray (EDX) spectra of a representative NAA-DBR with insets showing the percentage of main elements present before and after surface functionalization with TiO_2 (note: NAA-DBR produced with T_P = 1200 s and N_P = 150 pulses).

The inner surface of NAA-DBRs was coated with photoactive layers of TiO_2 by means of the sol-gel method. **Figure 3c** shows the energy dispersive X-ray (EDX) spectra with insets depicting the percentage of the elements present in as-produced (before sol-gel deposition) and TiO_2-functionalized (after sol-gel deposition) NAA-DBRs. The EDX spectra reveal that while the intensity of Al and S atoms are constant after the functional TiO_2 layers are deposited onto the NAA-DBRs, the intensity of O and Ti atoms increases. For instance, the relative percentage

of O, Al, S and Ti atoms in as-produced NAA-DBRs was 25, 70, 5, and 0%, respectively. Note that for this EDX spectrum, Al and O atoms correspond to alumina (Al_2O_3) while S atoms were incorporated into the structure of NAA from the acid electrolyte during anodization. After chemical modification of NAA-DBRs with TiO_2, the relative percentage of O, Al, S and Ti atoms were determined to be 37, 54, 5, and 4%, respectively. This analysis demonstrates the successful deposition of TiO_2 layers onto the inner surface of NAA-DBRs. The crystallographic phase of the TiO_2 layers under the synthesis conditions used in our study was amorphous (**Figure S3 – Supporting Information**).[4]

To summarize, modification of the anodization period can be used to precisely tune the optical properties (i.e. position of the PSB and interferometric color) of NAA-DBRs across the entire visible-NIR spectrum. Furthermore, the inner surface of NAA-DBRs can be functionalized with photoactive layers of TiO_2 through sol-gel method to create composite semiconductor PC structures for photocatalysis.

3.3. Assessment of Photocatalytic Degradation of Model Organic Molecules by TiO_2-NAA-DBRs. The photocatalytic performance of TiO_2-NAA-DBRs produced with varied T_P (i.e. from 900 to 1600 s with ΔT_P = 100 s) was assessed by investigating the photocatalytic degradation of three model pollutants (i.e. methyl orange – MO, rhodamine B – RhoB, and methylene blue – MB) under simulated solar light irradiation. **Figure S4 (Supporting Information)** displays the absorbance spectra of these organic molecules with the corresponding absorbance bands at 464, 554, and 664 nm, respectively. **Figure S5 (Supporting Information)** illustrates the simulated solar spectrum used in this study. Analysis of this spectrum reveals a spectral distribution of 0.12% UV (350–400 nm), 64.60% visible (400–750 nm) and 35.28% NIR (800–1025 nm). The photocatalytic reactions performed in this study are thus driven by visible-NIR light irradiation (i.e. 400–1025 nm), which is far from the characteristic energy bandgap of TiO_2 (i.e. 3.20–3.35 eV = 370–387 nm). Note that 100 mM

of H_2O_2 was added to the reaction solution to aid the photogeneration of charge carriers (e^-/h^+) in the photoactive TiO_2 layers deposited onto the inner surface of NAA-DBRs. The concentration of organic molecules with time in the reaction solution during the photo-driven degradation process (C_t) was estimated from the calibration lines shown in **Figure S1**. The photocatalytic performance of TiO_2-NAA-DBRs was fitted and calculated through the linearized pseudo-first order kinetics model shown in **Equation 2**:

$$-\ln(C_t/C_o) = kt \quad (2)$$

where C_o is the concentration after stirring in the dark for 30 min, C_t is the concentration at illumination time t, and k is the characteristic kinetic constant.

3.4. Effect of Anodization Period on Photocatalytic Degradation of MB. "Slow photons" are photons with reduced group velocity near the vicinity of the PSB of PCs. This effect increases the overall absorbance of the PC material, enhancing light–matter interactions for light harvesting since photons spend longer time within the photocatalytic material (i.e. generation of extra e^-/h^+ pairs for photocatalysis).[12,54] The well-defined and spectrally controllable PSB of TiO_2-NAA-DBRs make these PC structures excellent candidates to study and utilize these light-matter interactions at the nanoscale. Photocatalytic degradation of MB under simulated sunlight irradiation conditions was used as a model reaction to identify "slow photon" effects in TiO_2-NAA-DBRs fabricated with varying T_P from 900 to 1600 s, with ΔT_P = 100 s. **Figures 4a and b** and **Table 1** show the effect of T_P as a function of the relative position of the edges of the PSB of TiO_2-NAA-DBRs and the absorbance band of MB, using its photocatalytic degradation under simulated solar light irradiation as an indicator of "slow photon" enhancements. The kinetic constant (k) for TiO_2-NAA-DBRs with T_P = 900, 1000, 1100, 1200, 1300, 1400, 1500, and 1600 s were 1.83 ± 0.01, 2.00 ± 0.06, 2.80 ± 0.04, 3.04 ± 0.01, 2.63 ± 0.10, 2.22 ± 0.09, 2.77 ± 0.15, and 2.37 ± 0.08 h^{-1}, respectively (**Figure 4a** and **Table 1**). The highest k value was achieved by TiO_2-NAA-DBRs produced with T_P = 1200 s,

indicating that these composite semiconductor PCs provide the fastest and most efficient platform to photodegrade MB, with a 8–40% superior performance than that achieved by their counterparts produced with shorter or longer T_P. **Figure 4b** and **Table 1** indicate that the position of the red edge of the PSB of TiO_2-NAA-DBRs fabricated with T_P = 1200 s is the closest to the absorbance band of MB (i.e. $\lambda_{Abs\text{-}MB}$ = 664 nm) (i.e. ~17 nm away from the absorbance band maximum of MB). Upon irradiation, slow photons are strongly localized in the high (i.e. photoactive layer of TiO_2) and low (i.e. organic solution) dielectric parts of the red and blue edges of the characteristic PSB, respectively.[54] This phenomenon results in a longer lifetime of photons that increases the effective optical path length of the light waves when photons travel across the TiO_2-NAA-DBRs' structure. This enhanced light–matter interaction promotes the photon-to-electron conversion rate in these composite PC structures, speeding up the photocatalytic degradation of MB significantly when the edges of the PSB are located close to the absorbance band maximum of MB.[54-56] The "slow photon" effect is even more apparent when the red edge of the PSB is in the proximity of the absorbance band of MB. Here slow photons in that spectral region are strongly localized in the high refractive index region of the PC (i.e. semiconductor – TiO_2).[12,54] Our results confirm this hypothesis since this model photodegradation reaction is enhanced when the red edge of the PSB of TiO_2-NAA-DBRs is at its closest to the absorbance band maximum of MB.

The red edge of the PSB of TiO_2-NAA-DBRs produced with T_P = 1100 s is the second closest to the absorbance band maximum of MB (i.e. ~26 nm away). These PC structures are the second best performing type of TiO_2-NAA-DBR (i.e. $k = 2.80 \pm 0.04$ h^{-1}). This further confirms the hypothesis that the relative position of the red edge of the PSB with respect to the absorbance band of the organic model molecule plays a more significant role than that of the blue edge in enhancing the photocatalytic degradation of MB through "slow photon" effect. Although the red edge of the PSB of TiO_2-NAA-DBRs produced with T_P = 1300 s is the third

closest to the absorbance band maximum of MB (i.e. ~ 49 nm away), these PC platforms are slightly outperformed by TiO_2-NAA-DBRs fabricated with T_P = 1500 s, which achieve approximately 5% superior performance. **Figure 4b** shows that the characteristic PSB of TiO_2-NAA-DBRs produced with T_P = 1500 s partially overlaps with the absorbance band of MB, where the blue edge is 55 nm removed from the absorbance band maximum of MB. The red edge of the PSB of these PCs falls completely outside of the absorbance band. Since the blue edge of the PSB of these TiO_2-NAA-DBRs is located inside the absorbance band of MB, a partial enhancement of the photocatalytic performance due to "slow photon" effect is expected. However, since the PSB is practically located outside of the absorbance range of MB, photocatalytic enhancement under such a configuration relies strongly on other factors such as the geometric features of the overall PC structure. As indicated in **Table 1**, TiO_2-NAA-DBRs fabricated with T_P = 1500 s are produced with the second longest anodization time (i.e. t_{An} = 63.5 h), which is calculated from the number of anodization pulses (N_P = 150 pulses) and the anodization period (T_P = 1500 s) by **Equation 3**:

$$t_{An} = N_P/T_P \tag{3}$$

The total thicknesses or pore length (L_P – **Figure 1a**) of TiO_2-NAA-DBRs is directly proportional to the anodization time. An increase in total thicknesses of the PC platform enhances its overall light absorption, since more semiconductor matter is available for light–matter interactions.[41,57] This leads to the photogeneration of extra charge carriers (e^-/h^+) and thus to an enhancement of the photocatalytic activities achieved by those TiO_2-NAA-DBRs featuring thicker structure. The unexpectedly higher performance shown by TiO_2-NAA-DBRs produced with T_P = 1500 s is thus attributed to two contributing factors, a partial alignment of the blue edge of the PSB with respect to the absorbance band of MB and the total thickness of the PC platform. The fifth best performing TiO_2-NAA-DBRs platforms are those produced with T_P = 1600 s. These semiconductor PCs feature a PSB located almost entirely outside of

the absorbance range of MB. Despite having the longest t_{An} (i.e. 67.7 h), the photocatalytic performance shown by these TiO_2-NAA-DBRs is less efficient than that achieved by TiO_2-NAA-DBRs fabricated with T_P = 1500 s by ~14%. This result is attributable to the negligible contribution by "slow photon" effect to the photocatalytic performance since the blue edge of the PSB of these PCs is very far away from the absorbance band of MB (i.e. ~74 nm).

The blue edge of the PSB of TiO_2-NAA-DBRs fabricated with T_P = 1400 s is relatively close to the absorbance band maximum of MB (i.e. ~55 nm). However, these composite photonic structures provide the sixth best performance in degrading the model organic molecule (i.e. $k = 2.22 \pm 0.09$ h^{-1}). TiO_2-NAA-DBRs produced with T_P = 1400 s feature a thinner structure (i.e. t_{An} = 59.3 h) than that of those TiO_2-NAA-DBRs produced with T_P = 1500 and 1600 s (i.e. t_{An} = 63.5 and 67.7 h, respectively). This result is attributable to an inefficient combination of both "slow photon" effect and overall thickness of the PC structure, with a partial alignment of the PSB's blue edge and shorter pore length in the PC structure. The worst performing TiO_2-NAA-DBR structures have a T_P = 900 and 1000 s, with degradation rates $k = 2.00 \pm 0.06$ and 1.83 ± 0.01 h^{-1}, respectively. TiO_2-NAA-DBRs produced with T_P = 900 and 1000 s feature PSBs that are partially and entirely located within the absorbance range of MB, respectively. However, the red edge of the PSBs of these PCs is removed from the absorbance band maximum of MB (i.e. ~52 and 103 nm). Furthermore, these PCs have the thinnest structures (i.e. t_{An} = 38.5 and 42.7 h, respectively). Thus, a combination of a relative misalignment between the PSB's red edge and the thinnest PC structure has a significant detrimental effect on the overall photodegradation performance of these semiconductor PCs. This analysis establishes that the photocatalytic performance of TiO_2-NAA-DBRs with various T_P follows the order 1200 > 1100 > 1500 > 1300 > 1600 > 1400 > 1000 > 900 s. Changes in the characteristic color of the MB solution upon degradation by TiO_2-NAA-DBRs under simulated irradiation conditions, from 0 to 60 min with an interval of 15 min (**Figure S6 – Supporting Information**) also confirm the

photocatalytic degradation efficiency of TiO_2-NAA-DBRs by visual analysis. This result further demonstrates that MB molecules are efficiently photodegraded by TiO_2-NAA-DBRs after 1 h.

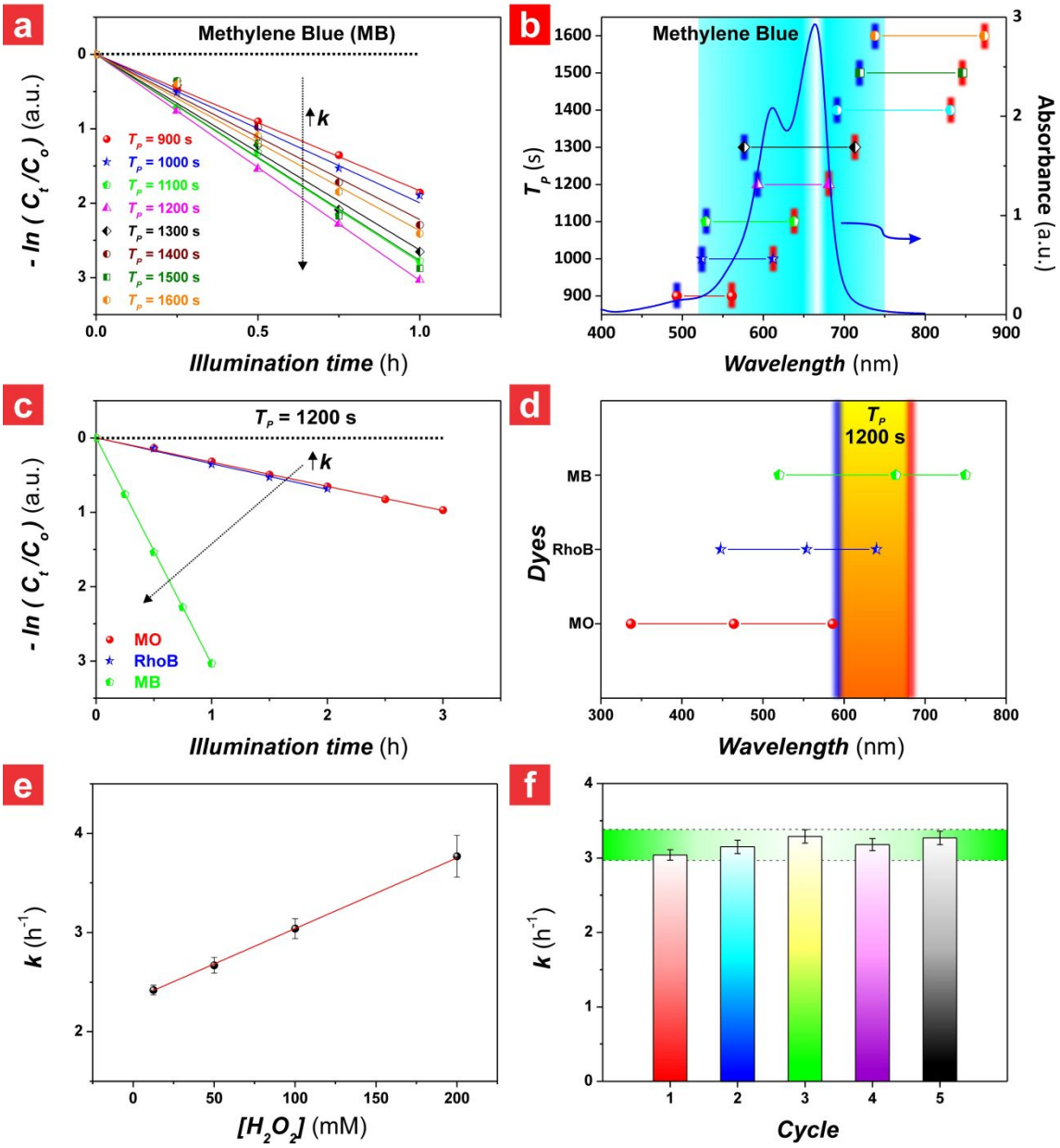

Figure 4. Photocatalytic assessment of TiO_2-NAA-DBRs as a function of anodization period (T_P), type of organic molecule, concentration of hydrogen peroxide (H_2O_2) solution, and recyclability (note: error bars in (a), (c), (e), and (f) correspond to standard deviation from n = 3 independent experiments). a) Photocatalytic degradation kinetics of methylene blue (MB) by TiO_2-NAA-DBRs produced with T_P from 900 to 1600 s with ΔT_P = 100 s under controlled irradiation conditions (note: black dotted line denotes the photodegradation of the corresponding organic in a control NAA-DBR fabricated without photoactive TiO_2 layers). b) Relative position of the blue and red edges of the characteristic photonic stopband (PSB) of TiO_2-NAA-DBRs from (a) with respect to the absorbance band of MB (note: white gap inside the absorbance band of MB denotes the band maximum of MB – $\lambda_{abs\text{-}MB}$ = 664 nm while blue and red vertical lines on the PSB correspond to the position of the blue and red edges of the PSB, respectively). c) Photocatalytic degradation kinetics of methyl orange (MO), rhodamine B (RhoB), and methylene blue (MB) by TiO_2-NAA-DBRs produced with T_P = 1200 s under controlled irradiation conditions (note: black dotted line denotes the photodegradation of the corresponding organic in a control NAA-DBR

fabricated without photoactive TiO_2 layers). d) Relative position of absorbance bands of model organics from (c) with the characteristic PSB of TiO_2-NAA-DBRs produced with T_P = 1200 s (note: the blue and red vertical lines on the PSB correspond to the position of the blue and red edges of the PSB, respectively). e) Linear correlation between the kinetic constant (k) and the concentration of H_2O_2 ([H_2O_2]) used in this study. f) Reusability test of TiO_2-NAA-DBRs produced with T_P = 1200 s on the photodegradation of MB under simulated solar light irradiation (note: horizontal bar corresponds to the standard deviation between the lowest and highest value of k).

Table 1. Effect of the relative position of the blue and red edges of the characteristic PSB and the total anodization time of TiO_2-NAA-DBRs fabricated with various T_P on the kinetic constant (k) for the photodegradation of MB molecules (note: error values correspond to standard deviation from n = 3 independent experiments).

Anodization Period (s)	**900**	**1000**	**1100**	**1200**	**1300**	**1400**	**1500**	**1600**
k (h^{-1})	1.83 ± 0.01	2.00 ± 0.06	2.80 ± 0.04	3.04 ± 0.01	2.63 ± 0.10	2.22 ± 0.09	2.77 ± 0.15	2.37 ± 0.08
Edge Nearest to the Peak	Red	Red	Red	Red	Red	Blue	Blue	Blue
Distance of Nearest Edge to the Peak (nm)	103	52	26	17	49	27	55	74
Total Anodization Time (h)	38.5	42.7	46.8	51.0	55.2	59.3	63.5	67.7

To summarize, the photocatalytic performance of TiO_2-NAA-DBRs is enhanced by the "slow photon" effect when the edges of the PSB fall within the absorbance range of MB. This enhancement is more significant when the red edge of the PSB of TiO_2-NAA-DBRs is at its closest to the absorbance band maximum of MB. Nevertheless, the thickness of the PC platform does play a more significant role in enhancing the photocatalytic properties of TiO_2-NAA-DBRs when the PSB is misaligned with the absorbance band of the model organic molecule. An optimum combination of relative position between the red edge of the PC's PSB and the thickness of the PC platform boosts photocatalytic reactions, making an efficient and rational utilization of the "slow photon" effect and the physical properties of these photocatalysts.

3.5. Effect of Type of Organic Molecule on the Photocatalytic Performance of TiO_2-NAA-DBRs. The effect of the type and characteristics of organic molecules on the photocatalytic

performance of TiO_2-NAA-DBRs was investigated by assessing the photocatalytic degradation of three model organics with well-defined absorbance bands across the visible spectral range (i.e. MO, RhoB, and MB). TiO_2-NAA-DBRs produced with T_P = 1200 s were used as photocatalyst platforms to study and identify "slow photon" effects associated with the relative position between the edges of the PCs' PSB and the absorbance and characteristics of the model organic molecules. **Figures 4c and d** and **Table 2** summarize the effect of the spectral arrangement between the absorbance bands of these model organic molecules and the position of the edges of the PSB of TiO_2-NAA-DBRs, using their respective photodegradation rate as an indicator of enhancements by "slow photon" effect. The k values for the photodegradation of MO, RhoB, and MB by TiO_2-NAA-DBRs produced with T_P = 1200 s were 0.32 ± 0.01, 0.35 ± 0.01, and 3.04 ± 0.01 h^{-1}, respectively (**Figure 4c**). The highest k value was achieved by the photodegradation of MB, which was degraded at a ~88 and 89% faster rate than RhoB and MO, respectively. As **Figure 4d** and **Table 2** indicate, the characteristic PSB of TiO_2-NAA-DBRs fabricated with T_P = 1200 s falls completely inside the absorbance range of MB. However, only the blue part of the PSB partially overlaps with the absorbance band of RhoB, and it is practically misaligned with the MO's absorbance range. The red edge of the PSB of these TiO_2-NAA-DBRs is located near the absorbance band of MB (i.e. ~17 nm away), while its blue edge is located within the range of the absorbance band of RhoB (i.e. ~39 nm away) and well-removed from the absorbance band of MO (i.e. ~129 nm away). As demonstrated in the previous section, the red edge of the PSB plays is more significant than the blue edge in enhancing photocatalytic reactions by "slow photon" effect. Our results confirm this hypothesis as indicated by the analysis of the relative positions of the red edge of the PC's PSB and the absorbance band of these model molecules.

It is worth noting that the charge of the organic molecule and its interaction with the surface charge of TiO_2-NAA-DBRs are also important contributing factors that impact on the overall

photodegradation rates achieved by these photocatalyst platforms. **Table S1 (Supporting Information)** collates the charge of the model organic molecules used in this study, where MO, RhoB, and MB are negatively, positively, and positively charged, respectively. The surface of the photoactive TiO_2 layer deposited onto the inner surface of NAA-DBRs is negatively charged at pH 5.5, the pH of the aqueous solution at which these photo-chemical reactions were performed. The negatively charged surface of TiO_2 would have high affinity for positively charged RhoB and MB molecules.[1,4] This would increase the total number of molecules adsorbed onto the surface of TiO_2, boosting the overall photocatalytic degradation rate of the system. Conversely, interaction between the negatively charged surface of the photoactive TiO_2 layers and negatively charged MO molecules is poor due to electrostatic repulsion. The reduced amount of MO molecules present within the vicinity of the photoactive layer would lead to a significant reduction of the system's performance. Another factor to consider is the intensity of the absorption bands of MO, RhoB, and MB. As **Figure S3** indicates, the absolute absorption intensity of MO, RhoB and MB at their central position maxima ($\lambda_{abs\text{-}MO}$ =464 nm, $\lambda_{abs\text{-}RhoB}$ = 554 nm, and $\lambda_{abs\text{-}MB}$ = 664 nm) are ~2.8, 3.6 and 1.5 a.u., respectively. RhoB (~3.6 a.u.) and MO (~2.8 a.u.) molecules absorb incoming light more efficiently than that MO (~1.5 a.u.). At these spectral regions, RhoB and MO molecules absorb most of the incoming light that propagates through the aqueous organic solutions before it reaches the surface of the TiO_2-NAA-DBRs. This screening effect reduces the overall photocatalytic performance of the material due to an inefficient use of photons in the semiconductor band. Therefore, overall photocatalytic degradation rates provided by TiO_2-NAA-DBRs are also dependent on the nature of the organic molecule, the electrostatic interactions surface-molecule and the relative positioning between the edges of the PSB and the absorbance band of the organics. These observations are in good agreement with our

previous study using NAA gradient-index filters as model photonic crystal platforms[4], which is a further evidence to support our conclusions.

Table 2. Values of the kinetic constant (k) for the photodegradation of three organics (i.e. MO, RhoB, and MB) by TiO_2-NAA-DBR with T_P = 1200 s (note: error values correspond to standard deviation from n = 3 independent experiments).

Organic Molecule	**MO**	**RhoB**	**MB**
$\boldsymbol{k}$ (h^{-1})	0.32 ± 0.01	0.35 ± 0.01	3.04 ± 0.01

3.6. Effect of Additive Concentration and Assessment of Reusability on the Photocatalytic Performance of TiO_2-NAA-DBRs. The relationship between the concentration of H_2O_2 ($[H_2O_2]$) and the photocatalytic degradation performance of TiO_2-NAA-DBRs was studied by assessing the photocatalytic degradation of MB by TiO_2-NAA-DBRs produced with T_P = 1200 s. In this experiment, the concentration of H_2O_2 was varied from 12.5, 50, 100 to 200 mM (**Figure 4e**). The kinetic constants for this photocatalytic reaction as a function of $[H_2O_2]$ were determined to be 2.42 ± 0.05, 2.67 ± 0.08, 3.04 ± 0.10, and 3.77 ± 0.21 h^{-1}, respectively. A linear fitting between the k values and $[H_2O_2]$ indicates that the former parameter increases with the latter at a rate of 0.01 ± 0.00 mM h^{-1}. This correlation can be associated with the higher number of $^{\cdot}OH$ radicals photogenerated in the inner surface of TiO_2-NAA-DBRs with increasing $[H_2O_2]$, which speed up the degradation of MB molecules. Reusability is another aspect of paramount importance to minimize the technological translation costs associated with the bench-to-field translation of photocatalyst materials. Reusability of TiO_2-NAA-DBRs was tested using the same TiO_2-NAA-DBR platform (i.e. T_P = 1200 s) in all five consecutive cycles of photodegradation, in which fresh MB solutions were photodegraded under simulated solar light irradiation for 1 h per cycle. The results summarized in **Figure 4f** show that k fluctuates from 3.04 ± 0.07 to 3.29 ± 0.09 h^{-1} between the first and fifth photodegradation cycle, demonstrating that TiO_2-NAA-DBRs provide a relatively similar performance after several

cycles of use. The average *k* value for the five photodegradation cycles is 3.18 ± 0.29 h^{-1}, where the photocatalytic conversion ratio of TiO_2-NAA-DBRs in the photodegradation of MB is ~96% under simulated solar light irradiation (**Table S2 – Supporting Information**). These results demonstrate that TiO_2-NAA-DBRs possess high photocatalytic activity, stability and reusability, which are required properties for real-life photocatalysis applications.

3.7. Assessment of Photocatalytic Degradation of 4-Chlorophenol by TiO_2-NAA-DBRs. Organic dyes are widely used model organics to assess the photocatalytic degradation performance of photocatalyst PC structures under visible light irradiation.[1,4-5,37] However, resilient organic pollutants such as pesticides have absorbance bands in the UV spectral region. This factor limits substantially the photocatalytic performance of PC structures with PSB in the visible range to degrade these chemicals under visible-NIR light irradiation. The ability of TiO_2-NAA-DBRs to degrade real-life resilient organic pollutants was assessed by studying the photodegradation of 4-chlorophenol (4-CP) under controlled visible-NIR irradiations conditions. 4-CP is used as intermediate in the production of pharmaceuticals, agricultural products, biocides, and paints and it is classified as a dangerous substance that can lead to irreversible changes in the aquatic ecosystems. 4-CP has a distinctive and well-resolved absorbance band located at 225 nm (**Figure S4 – Supporting Information**) to provide a direct relationship between its absorbance at 225 nm and the concentration of 4-CP in the solution as determined by the calibration line shown in **Figure S7 (Supporting Information)**. The effect of relative position of the blue and red edges of the PSB with the absorbance band of 4-CP on the photodegradation of 4-CP by TiO_2-NAA-DBRs was first studied using a set of TiO_2-NAA-DBRs fabricated with T_P = 900, 1200, and 1600 s as model PC platforms. **Figure 5a** shows dynamic photodegradation of 4-CP by these semiconductor PCs, while **Table 3** summarizes the kinetic constants estimated for TiO_2-NAA-DBRs produced with T_P = 900, 1200, and 1600 s calculated from linear fittings, which were 0.15 ± 0.01, 0.14 ± 0.01, and 0.03 ± 0.00 h^{-1},

respectively. These results indicate that TiO_2-NAA-DBRs produced with T_P = 900 and 1200 s provide the best photocatalytic performances, where the former model PCs showed a ~7% higher performance than that achieved by their equivalents produced with longer anodization period. In contrast, TiO_2-NAA-DBRs produced with T_P = 1600 s showed the worst photocatalytic performance, which was ~79 to ~80% worse than that of their 1200 and 900 s counterparts, respectively. **Figure 5b** shows the relative position of the edges of characteristic PSB of these semiconductor PCs with the absorbance band of 4-CP as a function of T_P. The PSB of all these TiO_2-NAA-DBRs falls completely outside of the absorbance range of 4-CP (**Figure S3**). Under such a configuration, the photocatalytic degradation of 4-CP by TiO_2-NAA-DBRs should not depend on the "slow photon" effect but rely solely upon the total thicknesses of TiO_2-NAA-DBR platforms. Therefore, the thicker the TiO_2-NAA-DBR platform the better the photocatalytic performance. However, the obtained k values indicate that the closer the PSB of TiO_2-NAA-DBRs is to the UV absorbance band of the model pesticide the faster the degradation rate achieved by this photocatalyst system (i.e. higher k value).

Table 3. Values of the kinetic constant (k) for the photodegradation of 4-CP by TiO_2-NAA-DBRs produced with T_P = 900, 1200, and 1600 s (note: error values correspond to standard deviation from n = 3 independent experiments).

Anodization Period (s)	**900**	**1200**	**1600**
$\boldsymbol{k}$ (h^{-1})	0.15 ± 0.01	0.14 ± 0.01	0.03 ± 0.00

This result is demonstrated to be independent on the thickness of the TiO_2-NAA-DBR platform (i.e. T_P = 900 s – t_{An} = 38.5 h; T_P = 1200 s – t_{An} = 51.0 h; T_P = 1600 s – t_{An} = 67.7 h). We hypothesize that this effect can be attributable to "slow photon" effect-driven enhancement of the photocatalysis performance achieved by these TiO_2-NAA-DBRs. **Figure 5b** further supports this hypothesis since the PSB of TiO_2-NAA-DBRs produced with T_P = 900 and 1200 s falls completely under the visible spectral region, while the PSB of TiO_2-NAA-DBRs fabricated with T_P = 1600 s is almost entirely located within the NIR region of the spectrum.

Figure S5 shows that ~65% of the artificial illumination used in our study corresponds to visible light, while the remaining ~35% of illumination is NIR light. Therefore, it is inferred that TiO_2-NAA-DBRs with PSB within the visible spectral region can collect and utilize more efficiently photons from the high irradiance visible region to generate carriers for photocatalytic degradation of 4-CP. This also contributes to the superior performance achieved by TiO_2-NAA-DBRs produced with shorter T_P, since the PSB of these PCs is located in the visible spectral range. Note that the overall photocatalytic degradation of 4-CP molecules is low as compared to that achieved for MO, RhoB, and MB. However, 4-CP is a chemically resilient and negatively charged molecule (**Table S1**) that is electrostatically repulsed by the negatively charged inner surface of TiO_2-NAA-DBRs. This minimizes the number of 4-CP molecules that are absorbed onto the photocatalyst platform surface, reducing the overall photodegradation performance of the system. Kim and Choi[58] studied the visible-light-induced degradation reaction of 4-CP in aqueous suspension, using pure TiO_2 powder as photocatalyst platform material. Their observations indicate that the surface complexation between phenolic compounds and TiO_2 appears to be responsible for the visible light reactivity. According to this photodegradation mechanism, a direct electron transfer from surface-complexed phenol groups to the conduction band of the TiO_2 coating upon absorbing visible light is the responsible factor to initiate the oxidative degradation of 4-CP.

The performances of photocatalyst materials are typically assessed using ultrapure water-based aqueous solutions. However, the effect of the composition and complexity of the aqueous matrix on the performance of photocatalysts is a critical aspect to consider for real-life applications and for the translation of fundamental advances in photocatalysis into practical systems that can address real-world problems. Therefore, the effect of the media composition on the photocatalytic performance of a set of TiO_2-NAA-DBRs produced with T_P = 1200 s was

assessed studying the degradation of 4-CP in various matrices (i.e. Milli-Q H_2O, tap H_2O, Torrens river H_2O, and 10 g L^{-1} NaCl aqueous solution).

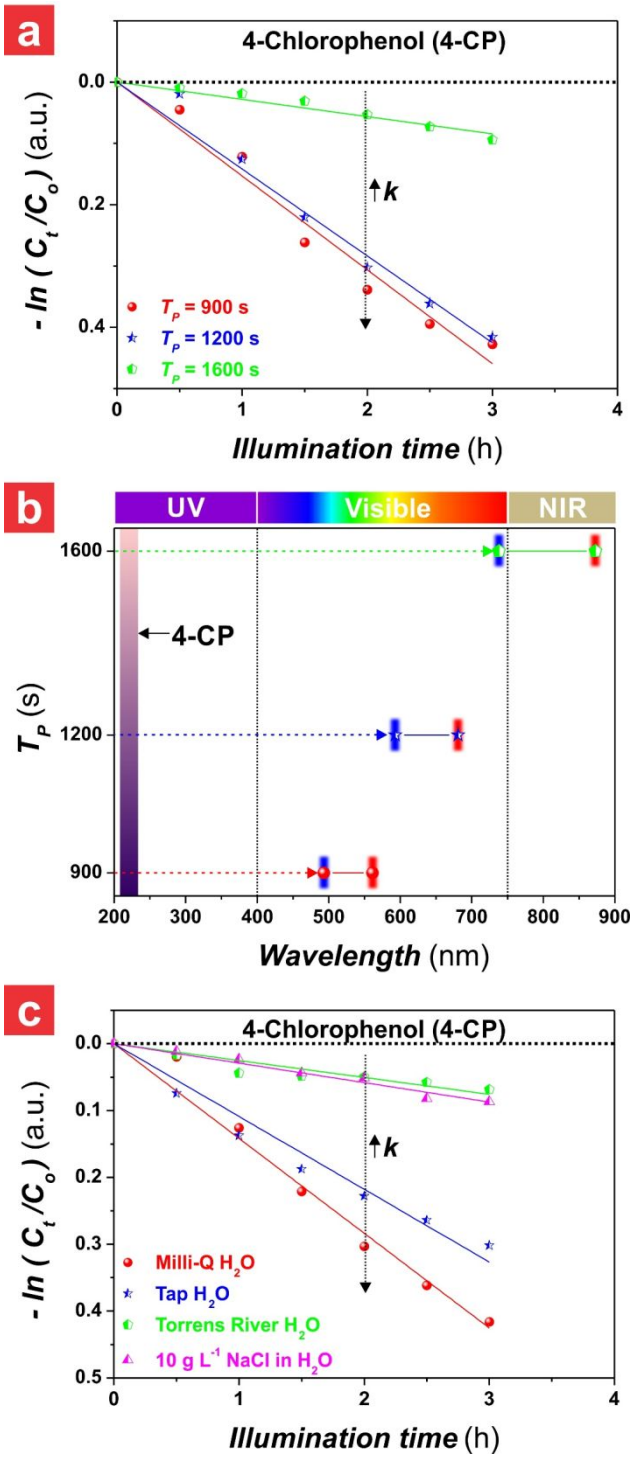

Figure 5. Photocatalytic assessment of TiO_2-NAA-DBRs on the photodegradation of 4-chlorophenol (4-CP) as a function of anodization period (T_P) and aqueous matrix composition (note: error bars in (a) and (c) correspond to standard deviation from n = 3 independent experiments). a) Photocatalytic degradation kinetics of 4-CP by TiO_2-NAA-DBRs produced with T_P = 900, 1200, and 1600 s under controlled irradiation conditions (note: black dotted

line denotes the photodegradation of the 4-CP in a control NAA-DBR fabricated without photoactive TiO_2 layers). b) Relative position of the blue and red edges of the characteristic photonic stopband (PSB) of TiO_2-NAA-DBRs from (a) with the absorbance band of 4-CP (note: the blue and red vertical lines on the PSB correspond to the position of the blue and red edges of the PSB, respectively). c) Photocatalytic degradation kinetics of 4-CP in different aqueous matrices by TiO_2-NAA-DBRs produced with T_P = 1200 s under controlled irradiation conditions (note: black dotted line denotes the photodegradation of 4-CP in a control NAA-DBR fabricated without photoactive TiO_2 layers).

Figure 5c shows dynamic photodegradation of 4-CP in these matrices and **Table 4** summarizes the obtained *k* values, which were estimated to be 0.14 ± 0.01, 0.11 ± 0.01, 0.025 ± 0.001, and 0.029 ± 0.002 h^{-1}, respectively. These results indicate that this photo-chemical reaction achieves its best performance when the aqueous matrix is Milli-Q H_2O (k = 0.14 ± 0.01 h^{-1}). This result is expected since this matrix does not have interfering molecules that can potentially hinder the interaction between 4-CP molecules and the inner functional surface of TiO_2-NAA-DBRs. The *k* value for the photodegradation of 4-CP in tap H_2O is the second highest and it was found to perform ~21% less efficiently than in Milli-Q H_2O under simulated solar light irradiation (k = 0.11 ± 0.01 h^{-1}). When the photocatalytic degradation of 4-CP is performed in environmental water from the Torrens river (Adelaide, Australia) and a Milli-Q H_2O-based 10 g L^{-1} NaCl solution, the *k* values were found to be ~73 and 81% lower than those obtained in less complex matrices (i.e. k = 0.025 ± 0.001 and 0.029 ± 0.002 h^{-1}, respectively). This result indicates that this photo-chemical reaction is hindered when it is conducted in complex matrices. This significant difference in photocatalytic degradation of 4-CP by TiO_2-NAA-DBRs can be attributable to interfering ions and molecules present in these complex solutions.

Table 4. Values of the kinetic constant (*k*) for the photodegradation of 4-CP in four different matrices (i.e. Milli-Q H_2O, tap H_2O, Torrens river H_2O, and 10 g L^{-1} NaCl aqueous solution) by TiO_2-NAA-DBRs produced with T_P = 1200 s (note: error values correspond to standard deviation from n = 3 independent experiments).

Matrix	**Milli-Q H_2O**	**Tap H_2O**	**Torrens river H_2O**	**10 g L^{-1} NaCl**
k (h^{-1})	0.14 ± 0.01	0.11 ± 0.00	0.025 ± 0.001	0.029 ± 0.002

Milli-Q H_2O and tap H_2O matrices are relatively free from ions and molecules, although the latter contains some small concentration of ions such as Ca^{2+}, Na^{+}, K^{+}, Mg^{2+}, Fe^{2+}, and Cl^{-} that

slightly interfere with the photodegradation of 4-CP, as indicated by the *k* values. When this light-driven reaction is performed in a saline aqueous solution (i.e. 10 g L^{-1} NaCl), salt molecules dissociate in water to form Na^+ and Cl^- ions. A high concentration of these ions inside the nanopores of TiO_2-NAA-DBRs is demonstrated to slow down this reaction by hindering interactions between the inner surface of TiO_2-NAA-DBRs and water molecules to form ·OH radicals that subsequently oxidize absorbed 4-CP molecules into bi-products. Furthermore, presence of these ions also reduces the total amount of 4-CP molecules absorbed onto the negatively charged inner surface of TiO_2-NAA-DBRs, decreasing significantly the overall performance of the system. As the *k* values indicate, the photocatalytic degradation of 4-CP in Torrens river H_2O is slightly worse than that obtained in the 10 g L^{-1} NaCl aqueous solution, due to the presence of ions and organic molecules that interfere the formation of ·OH radicals and compete with the absorption of 4-CP molecules onto the inner surface of TiO_2-NAA-DBRs. This analysis reveals that the photocatalytic performance of TiO_2-NAA-DBRs in degrading 4-CP molecules is thus highly affected by the presence of interfering ions and organic molecules. However, TiO_2-NAA-DBRs are still efficient enough to degrade a highly resilient environmental pollutant in complex aqueous matrices. This is a clear demonstration of the potential of these semiconductor PC structures for real-life applications.

3.8. Photocatalytic Degradation Mechanism. The experimental results obtained in this study allow us to propose a photocatalytic degradation mechanism that explains the performance of TiO_2-NAA-DBRs. These NAA-based PC structures collect photons from high irradiance spectral region (i.e. visible and NIR), which are efficiently utilized by the photoactive TiO_2 layers to speed up photocatalytic reaction rates, as indicated by the degradation of model organic molecules. In this process, charge carriers (e^-/h^+) are generated and separated upon light irradiation to the conduction band and valence band of TiO_2, respectively. These charge carriers are subsequently transferred to the surroundings of the nanopores' surface and react

with redox species to produce reactive oxidation species (i.e. ·OH radicals), which decompose organic molecules absorbed onto or close to the inner surface of the nanopores.[59] When H_2O_2 molecules are added to the matrix solution, electrons at the conduction band react with H_2O_2 to form ·OH radicals and $^-$OH ions, which can be further oxidized to ·OH radicals by the photogenerated holes at the valence band of TiO_2. Photogenerated holes also oxidize H_2O molecules to form ·OH radicals, which decompose organic molecules into CO_2 and H_2O, which are harmless to the environment. Our results demonstrate that the photocatalytic decomposition rate at the TiO_2 layers can be significantly enhanced by rationally engineering the underlying NAA-DBR structure to increase photon-to-electron conversion rates at the TiO_2 functional layers. Photons absorbed by the structure of NAA-DBRs propagate with reduced group velocity and localize near the PSB's edges, resulting in longer lifespan of photons at these spectral regions. These photons can be subsequently utilized by the photoactive TiO_2 layers to generate extra carriers and accelerate light-driven redox reactions occurring within the nanopores of TiO_2-NAA-DBRs. The "slow photon" effect is strongly dependent on the relative position of the PSB's edges with respect to the absorbance band of model organic molecules. For instance, the photocatalytic enhancement was found to be maximum when the PSB's red edge falls completely within the absorbance band maximum of the organic molecules. Our results also indicate that positioning the blue edge of the PSB towards the absorbance band maximum of these organic molecules can enhance photocatalytic reactions by "slow photon" effect too, although in a less efficient manner than that achieved by the red edge due to the higher localization of slow photons at the high refractive index section of the PC structure (i.e. semiconductor – red edge).

The "slow photon" enhancement is dramatically reduced when the distance between the PSB's edges and the absorbance band of organic molecules is increased. Under this arrangement (i.e. partial overlapping between the PC's PSB and the absorbance band of the organic molecule),

the contribution of the "slow photon" effect to the overall photocatalytic enhancement is weak, and other factors such as the total pore length of the composite PC structure are found to have a more significant contribution towards the photocatalytic performance of the PC structure. However, the assessment on the photodegradation of 4-CP molecules (i.e. absorbance band in the UV range) indicates that, when the configuration of the system is such that the PSB falls completely outside the absorbance band of the organic molecule, the closer the PSB is from the absorbance band the more efficient the photocatalytic PC system is, independently of its overall thickness. However, other factors such as percentage of high irradiance spectral regions also contribute significantly to the overall performance of these semiconductor PCs. Our study also establishes that the nature of the organic molecule is another important contributing factor to the efficiency of these light-driven reactions.

3.9. Comparative Analysis with Benchmark Photocatalyst Platforms. Table 5 compiles a summary of representative studies using benchmark photocatalyst materials with and without PC structure, the performance of which was assessed under visible light irradiation conditions. Multiple studies reported on the photocatalytic performance of P25 TiO_2 nanoparticles to photodegrade MO, RhoB, MB, and 4-CP under visible light irradiation conditions.[1,60] P25 TiO_2 is a benchmark photocatalyst material that features anatase crystallographic phase and only absorbs light in the UV spectral region. The photocatalytic degradation rates reported for P25 TiO_2 nanoparticles when photodegrading these model organics were k_{MO} = 0.00 h^{-1}, k_{RhoB} = 0.17 h^{-1}, k_{MB} = 0.64 h^{-1}, and $k_{4\text{-}CP}$ = 0.0037 h^{-1}. These values indicate that TiO_2-NAA-DBRs substantially outperform P25 TiO_2 nanoparticles in the degradation of these organic molecules under visible light irradiation, with a photocatalytic enhancement of 100, 51, 79, and 75%, respectively. Though a direct comparison could not be entirely correct due to differences in experimental conditions (e.g. irradiation spectral distribution, power density, catalyst loading,

etc.), this comparison indicates the potential of TiO_2-NAA-DBRs as efficient photocatalyst platforms.

Table 5. Compilation of representative kinetic constant (k) values for the photodegradation of MO, RhoB, MB, and 4-CP molecules by various photocatalysts.

Photocatalyst	k (h^{-1})				Ref.
	MO	RhoB	MB	4-CP	
P25 TiO_2 Nanoparticles	0.00	0.17	0.64	0.037	1, 60
TiO_2 Inverse Opal	0.01	0.47	1.32	-	1
ZnO Inverse Opal	0.01	0.13	1.49	0.00	30
TiO_2-NAA-GIFs	0.25	0.39	2.10	-	4
TiO_2-NAA-DBRs	0.32	0.35	3.04	0.15	This Study

TiO_2 inverse opals feature a 3D PC structure and have been devised as promising photocatalyst platforms due to their well-defined and relatively controllable characteristic PSB. The PC structure of semiconductor inverse opals enables the utilization of the "slow photon" effect to enhance photocatalytic reactions. Zheng *et al.*[1] fabricated a set of TiO_2-based inverted opal structures featuring various pore sizes (i.e. from 270 to 550 nm) and assessed the photodegradation of three model organic dyes (i.e. RhoB, MO, and MB) under visible light irradiation. The photocatalytic performance achieved by this system was k_{MO} = 0.01 h^{-1}, k_{RhoB} = 0.47 h^{-1}, and k_{MB} = 1.32 h^{-1}, respectively. Although these TiO_2 inverse opal structures outperform TiO_2-NAA-DBRs by ~34% in the photodegradation of RhoB, TiO_2-NAA-DBRs show enhanced photocatalytic performances in the photodegradation of MO and MB (i.e. ~97 and ~57% superior performance, respectively). Other types of inverse opal PC structures have been explored for enhanced photon-to-electron conversion rates through the "slow photon" effect. For instance, ZnO-based inverse opals with PSB positioned in the visible range (i.e. 510,

600, and 720 nm) were fabricated by systematically modifying the pore size of the semiconductor structure from 260 to 320 nm. The photocatalytic performance of these PCs was assessed by the degradation of MO, RhoB, MB, and 4-CP under visible light irradiation.[30] These ZnO inverse opal structures achieved photocatalytic degradation rates of $k_{MO} = 0.01\ h^{-1}$, $k_{RhoB} = 0.13\ h^{-1}$, $k_{MB} = 1.49\ h^{-1}$, and $k_{4\text{-}CP} = 0.00\ h^{-1}$ for MO, RhoB, MB, and 4-CP molecules, respectively. A comparison with our results (**Table 5**) indicates that TiO_2-NAA-DBR structures provide superior properties than ZnO inverse opals to photodegrade these organic molecules, with an enhancement of 97, 63, 51, and 100%, respectively.

Our group developed NAA-based gradient-index filters (NAA-GIFs) PC structures with deposited photoactive layers of TiO_2.[4] TiO_2-NAA-GIFs were produced with varying anodization period (i.e. from 650 to 850 s) and used as photocatalyst platforms to degrade MO, RhoB, and MB under visible-NIR irradiation. The photocatalytic decomposition rates achieved for MO, RhoB, and MB were $k_{MO} = 0.25\ h^{-1}$, $k_{RhoB} = 0.39\ h^{-1}$, and $k_{MB} = 2.10\ h^{-1}$, respectively. Although the photocatalytic performance of TiO_2-NAA-GIFs for RhoB was 11% better than that achieved by TiO_2-NAA-DBRs, TiO_2-NAA-DBRs show more efficient performance for MO and MB, with an enhancement of 22 and 31%, respectively. In general, TiO_2-NAA-DBRs perform more efficiently than TiO_2-NAA-GIFs under visible-NIR irradiation. This enhancement may be attributable to the more efficient light collection associated with the broader and intense characteristic PSB of NAA-DBR structures.

To summarize, this comparison demonstrates that the photocatalytic performance of TiO_2-NAA-DBRs is generally superior to that of existing photocatalyst systems. The optical and optoelectronic properties of these semiconductor composite PC structures can be precisely tuned across the spectral regions to achieve enhanced performances in photocatalysis by rationally managing photons at the nanoscale.

CONCLUSIONS

This study provides new insights into the capability of NAA-based composite semiconductor photonic crystal structures to enhance and accelerate photocatalytic reactions by the "slow photon" effect. NAA-DBRs with varying anodization period were fabricated by stepwise pulse anodization and subsequently functionalized with photoactive TiO_2 layers. The optical properties of these model nanoporous semiconductor PCs can be precisely tuned across the spectral regions to identify light–matter interactions that lead to unprecedented enhancements in photocatalytic reactions. "Slow photon" effects in TiO_2-NAA-DBRs were investigated by model photo-chemical reactions, using the photodegradation of methyl orange, rhodamine B, methylene blue, and 4-chlorophenol under controlled visible-NIR light irradiation. Our study demonstrates that TiO_2-NAA-DBRs degrade these organic molecules efficiently with high photocatalytic performances (i.e. $k_{MO} = 0.32 \pm 0.01$ h^{-1}, $k_{RhoB} = 0.35 \pm 0.01$ h^{-1}, $k_{MB} = 3.04 \pm 0.01$ h^{-1} and $k_{4\text{-}CP} = 0.15 \pm 0.01$ h^{-1}). TiO_2-NAA-DBRs demonstrate outstanding photocatalytic performances as compared to other benchmark photocatalyst platforms such as P25 TiO_2 nanoparticles and TiO_2 and ZnO inverted opal PCs.

Enhancement of photodegradation rates in TiO_2-NAA-DBRs is found to be optimal when the red edge of the PSB is in close proximity to or falls entirely within the absorbance band of the model organic molecules. However, the photocatalytic enhancement by the "slow photon" effect becomes weaker with increasing distance between the edges of the PSB and the absorbance band of the organic molecules. When the PSB partially overlaps with the absorbance band of the organic compound, a compromise between the total pore length of the PC structure and the "slow photon" effect in the photocatalytic enhancement can provide photocatalytic enhancements by an optimal combination of these factors. Our study also indicates that, in the case of organics with absorbance bands in the UV spectral region, when the PC's PSB is in the visible or NIR regions, the photocatalytic performance of TiO_2-NAA-DBRs is only associated with the relative distance between the absorbance band and the PC's

PSB and the percentage of visible-NIR irradiation, and independent on the total pore length of the PC structure. Furthermore, our study demonstrates that interferences from ions and molecules present in the aqueous matrix strongly decrease the overall photocatalytic degradation rate of TiO_2-NAA-DBRs. However, these PC structures are still able to photodegrade resilient pesticide molecules such as 4-chlorophenol in complex aqueous matrices. The charge of the organic molecules and the concentration of hydrogen peroxide solution are also contributing factors in dictating the overall photocatalytic performance of TiO_2-NAA-DBRs, where positively charged molecules (i.e. rhodamine B and methylene blue) and higher concentration of hydrogen peroxide result in enhanced photocatalytic performances. TiO_2-NAA-DBRs also provide high photostability and reusability in the photocatalytic degradation of organic molecules and can maintain their outstanding performance after five cycles.

In summary, this study provides new opportunities to develop sustainable and high-performing photocatalyst platforms based on surface-functionalized nanoporous anodic alumina photonic crystals fabricated with a rational design of optical properties to attain an efficient management of photons for photocatalysis.

AUTHORS INFORMATION

Corresponding Authors

Professor Lluís F. Marsal

Department of Electronic, Electric, and Automatics Engineering – Universitat Rovira i Virgili

Phone: + 34 977559625

Email: lluis.marsal@urv.cat

Web page: http://www.urv.cat/html/docencia-per-centre/general-94602760.php

Professor Nicolas H. Voelcker

Monash Institute of Pharmaceutical Sciences – Monash University

Phone: + 61 03 9902 9097

Email: nicolas.voelcker@monash.edu

Web page: https://research.monash.edu/en/persons/nicolas-voelcker

Professor Andrew Abell

School of Chemistry and Physics – The University of Adelaide

Phone: + 61 8 8313 5652

Email: andrew.abell@adelaide.edu.au

Web page: http://researchers.adelaide.edu.au/profile/andrew.abell#contact-details

Doctor Abel Santos

School of Chemical Engineering – The University of Adelaide

Phone: +61 8 8313 1535

Email: abel.santos@adelaide.edu.au

Web page: http://www.adelaide.edu.au/directory/abel.santos

Notes

The authors declare no competing financial interest.

ACKNOWLEDGMENT

Authors thank the support provided by the Australian Research Council (ARC) through the grant number CE140100003, the School of Chemical Engineering, the University of Adelaide (DVCR 'Research for Impact' initiative), the Institute for Photonics and Advanced Sensing (IPAS), the ARC Centre of Excellence for Nanoscale BioPhotonics (CNBP), the Spanish Ministry of Economy and competitiveness TEC2015-71324-R (MINECO/FEDER), the Catalan authority AGAUR 2017SGR1527, and ICREA under the ICREA Academia Award. This work was performed in part at the Melbourne Centre for Nanofabrication (MCN) in the Victorian Node of the Australian National Fabrication Facility (ANFF).

ASSOCIATED CONTENT

Supporting Information. Further information on the fabrication, surface functionalization and photocatalytic performance of TiO_2-NAA-DBRs; the calibration lines correlating organic molecules concentration and absorbance; transmission spectra of NAA-DBRs; absorbance

spectra of organic molecules; spectrum for the simulated solar light irradiation; digital pictures of photodegraded MB solution; properties of organic molecules; results of reusability. This material is available free of charge via the Internet at http://pubs.acs.org.

REFERENCES

1. Zheng, X.; Meng, S.; Chen, J.; Wang, J.; Xian, J.; Shao, Y.; Fu, X.; Li, D. Titanium Dioxide Photonic Crystals with Enhanced Photocatalytic Activity: Matching Photonic Band Gaps of TiO_2 to the Absorption Peaks of Dyes. *J. Phys. Chem. C* **2013**, *117*, 21263-21273.

2. Geng, Z.; Zhang, Y.; Yuan, X.; Huo, M.; Zhao, Y.; Lu, Y.; Qiu, Y. Incorporation of Cu_2O nanocrystals into TiO_2 Photonic Crystal for Enhanced UV-Visible Light Driven Photocatalysis. *J. Alloys Compd.* **2015**, *644*, 734-741.

3. Lu, Y.; Yu, H.; Chen, S.; Quan, X.; Zhao, H. Integrating Plasmonic Nanoparticles with TiO_2 Photonic Crystal for Enhancement of Visible-Light Driven Photocatalysis. *Environ. Sci. Technol.* **2012**, *46*, 1724-1730.

4. Lim, S. Y.; Law, C. S.; Markovic, M.; Kirby, J. K.; Abell, A. D.; Santos, A. Engineering the Slow Photon Effect in Photoactive Nanoporous Anodic Alumina Gradient-Index Filters for Photocatalysis. *ACS Appl. Mater. Interfaces* **2018**, *10*, 24124-24136.

5. Toumazatou, A.; Arfanis, M. K.; Pantazopoulos, P.-A.; Kontos, A. G.; Falaras, P.; Stefanou, N.; Likodimos, V. Slow-Photon Enhancement of Dye Sensitized TiO_2 Photocatalysis. *Mater. Lett.* **2017**, *197*, 123-126.

6. Sheng, X.; Liu, J.; Coronel, N.; Agarwal, A. M.; Michel, J.; Kimerling, L. C. Integration of Self-Assembled Porous Alumina and Distributed Bragg Reflector for Light Trapping in Si Photovoltaic Devices. *IEEE Photonics Technol. Lett.* **2010**, *22*, 1394-1396.

7. Guo, M.; Xie, K.; Wang, Y.; Zhou, L.; Huang, H. Aperiodic TiO_2 Nanotube Photonic Crystal: Full-Visible-Spectrum Solar Light Harvesting in Photovoltaic Devices. *Sci. Rep.* **2014**, *4*, 6442.

8. Guo, M.; Su, H.; Zhang, J.; Liu, L.; Fu, N.; Yong, Z.; Huang, H.; Xie, K. Broadband and Omnidirectional Light Harvesting Enhancement in Photovoltaic Devices with Aperiodic TiO_2 Nanotube Photonic Crystal. *J. Power Sources* **2017**, *345,* 12-20.

9. Dronov, R.; Jane, A.; Shapter, J. G.; Hodges, A.; Voelcker, N. H. Nanoporous Alumina-Based Interferometric Transducers Ennobled. *Nanoscale* **2011**, *3*, 3109-3114.

10. Wijnhoven, J. E. G. J.; Vos, W. L. Preparation of Photonic Crystals Made of Air Sphers in Titania. *Science* **1998**, *281*, 802-804.

11. Yablonovitch, E. Inhibited Spontaneous Emission in Solid-State Physics and Electronics. *Phys. Rev. Lett.* **1987**, *58*, 2059.

12. Liu, J.; Zhao, H.; Wu, M.; Van der Schueren, B.; Li, Y.; Deparis, O.; Ye, J.; Ozin, G. A.; Hasan, T.; Su, B.-L. Slow Photons for Photocatalysis and Photovoltaics. *Adv. Mater.* **2017**, *29*, 1605349.

13. Guesh, K.; Márquez-Álvarez, C.; Chebude, Y.; Diaz, I. Enhanced Photocatalytic Activity of Supported TiO_2 by Selective Surface Modification of Zeolite Y. *Appl. Surf. Sci.* **2016**, *378*, 473-478.

14. Wang, C.; Shi, H.; Li, Y. Synthesis and Characteristics of Natural Zeolite Supported Fe^{3+}-TiO_2 Photocatalysts. *Appl. Surf. Sci.* **2011**, *257*, 6873-6877.

15. Dong, H.; Zeng, G.; Tang, L.; Fan, C.; Zhang, C.; He, X.; He, Y. An Overview on Limitations of TiO_2-Based Particles for Photocatalytic Degradation of Organic Pollutants and the Corresponding Countermeasures. *Water Res.* **2015**, *79*, 128-146.

16. Zhu, X.; Chang, Y.; Chen, Y. Toxicity and Bioaccumulation of TiO_2 Nanoparticle Aggregates in Daphnia Magna. *Chemosphere* **2010**, *78*, 209-215.

17. Hoffman, M. R.; Martin, S. T.; Choi, W.; Bahnemann, D. W. Environmental Applications of Semiconductor Photocatalysis. *Chem. Rev.* **1995**, *95*, 69-96.

18. Chen, X.; Shen, S.; Guo, L.; Mao, S. S. Semiconductor-based Photocatalytic Hydrogen Generation. *Chem. Rev.* **2010**, *110*, 6503-6570.

19. Liu, G.; Wang, L.; Yang, H. G.; Cheng, H.-M.; Lu, G. Q. Titania-Based Photocatalysts – Crystal Growth, Doping and Heterostructuring. *J. Mater. Chem.* **2010**, *20*, 831-843.

20. Ollis, D. F.; Pelizzetti, E.; Serpone, N. Photocatalyzed Destruction of Water Contaminants. *Environ. Sci. Technol.* **1991**, *25*, 1522-1529.

21. Liu, J.; Liu, G.; Li, M.; Shen, W.; Liu, Z.; Wang, J.; Zhao, J.; Jiang, L.; Song, Y. Enhancement of Photochemical Hydrogen Evolution over Pt-Loaded Hierarchical Titania Photonic Crystal. *Energy Environ. Sci.* **2010**, *3*, 1503-1506.

22. Kim, K.; Thiyagarajan, P.; Ahn, H.-J.; Kim, S.-I.; Jang, J.-H. Optimization for Visible Light Photocatalytic Water Splitting: Gold-Coated and Surface-Textured TiO_2 Inverse Opal Nano-Networks. *Nanoscale* **2013**, *5*, 6254-6260.

23. Boppella, R.; Kochuveedu, S. T.; Kim, H.; Jeong, M. J.; Mota, F. M.; Park, J. H.; Kim, D. H. Plasmon-Sensitized Graphene/TiO_2 Inverse Opal Nanostructures with Enhanced Charge Collection Efficiency for Water Splitting. *ACS Appl. Mater. Interfaces* **2017**, *9*, 7075-7083.

24. Zhou, M.; Bao, J.; Xu, Y.; Zhang, J.; Xie, J.; Guan, M.; Wang, C.; Wen, L.; Lei, Y.; Xie, Y. Photoelectrodes Based Upon Mo:$BiVO_4$ Inverse Opals for Photoelectrochemical Water Splitting. *ACS Nano* **2014**, *8*, 7088-7098.

25. Sadakane, M.; Sasaki, K.; Kunioku, H.; Ohtani, B.; Abe, R.; Ueda, W. Preparation of 3-D Ordered Macroporous Tungsten Oxides and Nano-Crystalline Particulate Tungsten Oxides Using a Colloidal Crystal Template Method, and Their Structural Characterization and Application as Photocatalysts under Visible Light Irradiation. *J. Mater. Chem.* **2010**, *20*, 1811-1818.

26. Hirakawa, H.; Hashimoto, M.; Shiraishi, Y.; Hirai, T. Photocatalytic Conversion of Nitrogen to Ammonia with Water on Surface Oxygen Vacancies of Titanium Dioxide. *J. Am. Chem. Soc.* **2017**, *139*, 10929-10936.

27. Jiao, J.; Wei, Y.; Chi, K.; Zhao, Z.; Duan, A.; Liu, J.; Jiang, G.; Wang, Y.; Wang, X.; Han, C.; Zheng, P. Platinum Nanoparticles Supported on TiO_2 Photonic Crystals as Highly Active Photocatalyst for the Reduction of CO_2 in the Presence of Water. *Energy Technol.* **2017**, *5*, 877-883.

28. Ren, M.; Valsaraj, K. Inverse Opal Titania on Optical Fiber for the Photoreduction of CO_2 to CH_3OH. *Int. J. Chem. React. Eng.* **2009**, *7*, A90.

29. Fox, M. A.; Dulay, M. T. Heterogeneous Photocatalysis. *Chem Rev.* **1993**, *93*, 341-357.

30. Meng, S.; Li, D.; Wang, P.; Zheng, X.; Wang, J.; Chen, J.; Fang, J.; Fu, X. Probing Photonic Effect on Photocatalytic Degradation of Dyes Based on 3D Inverse Opal ZnO Photonic Crystal. *RSC Adv.* **2013**, *3*, 17021-17028.

31. Xie, H.; Li, Y.; Jin, S.; Han, J.; Zhao, X. Facile Fabrication of 3D-Ordered Macroporous Nanocrystalline Iron Oxide Films with Highly Efficient Visible Light Induced Photocatalytic Activity. *J. Phys. Chem. C* **2010**, *114*, 9706-9712.

32. Li, X.; Chen, Z.; Quan, H.; Shao, Y.; Li, D. Constructing Photocatalyst from β-Bi_2O_3 Photonic Crystals for Enhanced Photocatalytic Performance. *J. Porous Mater.* **2018**, *25*, 677-685.

33. Curti, M.; Schneider, J.; Bahnemann, D. W.; Mendive, C. B. Inverse Opal Photonic Crystals as a Strategy to Improve Photocatalysis: Underexplored Questions. *J. Phys. Chem. Lett.* **2015**, *6*, 3903-3910.

34. Stein, A.; Wilson, B. E.; Rudisill, S. G. Design and Functionality of Colloidal-Crystal-Templated Materials – Chemical Applications of Inverse Opals. *Chem. Soc. Rev.* **2013**, ***42***, 2763-2803.

35. Gaillot, D. P.; Summers, C. J. Inverse Opal Photonics. In *Atomic Layer Deposition of Nanostructured Materials*; Pinna, N., Knez, M., Eds.; Wiley-VCH: Weinheim, 2012; pp. 345-371.

36. Likodimos, V. Photonic Crystal-Assisted Visible Light Activated TiO_2 Photocatalysis. *Appl. Catal. B* **2018**, *230*, 269-303.

37. Zhai, C.; Zhu, M.; Lu, Y.; Ren, F.; Wang, C.; Du, Y.; Yang, P. Reduced Graphene Oxide Modified Highly Ordered TiO_2 Nanotube Arrays Photoelectrode with Enhanced Photoelectrocatalytic Performance under Visible-Light Irradiation. *Phys. Chem. Chem. Phys.* **2014**, *16*, 14800-14807.

38. Liao, W.; Yang, J.; Zhou, H.; Murugananthan, M.; Zhang, Y. Electrochemically Self-Doped TiO_2 Nanotube Arrays for Efficient Visible Light Photoelectrocatalytic Degradation of Contaminants. *Electrochim. Acta* **2014**, *136*, 310-317.

39. Wang, C.; Chen, D.; Ping, G. X.; Liu, S.; Huang, X. N.; Huang, Y. X.; Shu, K. Y.; Li, J. H. Controllable Synthesis of Well-Ordered TiO_2 Nanotubes in a Mixed Organic Electrolyte for High-Efficiency Photocatalysis. *Sci. China Chem.* **2012**, *55*, 2373-2380.

40. Mehedi, I. M.; Hossain, M. F.; Takahashi, T.; Islam, M. S. Nano-Structural Variation of Highly Aligned Anodic Titania Nanotube Arrays for Gas Phase Photocatalytic Application. *J. Photochem. Photobiol. A* **2017**, *335*, 200-210.

41. Santos, A.; Balderrama, V. S.; Alba, M.; Formentín, P.; Ferré-Borrull, J.; Pallarès, J.; Marsal, L. F. Nanoporous Anodic Alumina Barcodes: Toward Smart Optical Biosensors. *Adv. Mater.* **2012**, *24*, 1050-1054.

42. Law, C. S.; Sylvia, G. M.; Nemati, M.; Yu, J.; Losic, D.; Abell, A. D.; Santos, A. Engineering of Surface Chemistry for Enhanced Sensitivity in Nanoporous Interferometric Sensing Platforms. *ACS Appl. Mater. Interfaces* **2017**, *9*, 8929-8940.

43. Law, C. S.; Lim, S. Y.; Abell, A. D.; Santos, A. Real-Time Binding Monitoring between Human Blood Proteins and Heavy Metal Ions in Nanoporous Anodic Alumina Photonic Crystals. *Anal. Chem.* **2018**, *90*, 10039-10048.

44. Chen, Y.; Santos, A.; Wang, Y.; Kumeria, T.; Wang, C.; Li, J.; Losic, D. Interferometric Nanoporous Anodic Alumina Photonic Coatings for Optical Sensing. *Nanoscale* **2015**, *7*, 7770-7779.

45. Law, C.S.; Lim, S. Y.; Santos, A. On the Precise Tuning of Optical Filtering Features in Nanoporous Anodic Alumina Distributed Bragg Reflectors. *Sci. Rep.* **2018**, *8*, 4642.

46. Santos, A.; Pereira, T.; Law, C. S.; Losic, D. Rational Engineering of Nanoporous Anodic Alumina Optical Bandpass Filters. *Nanoscale* **2016**, *8*, 14846-14857.

47. Wang, Y.; Chen, Y.; Kumeria, T.; Ding, F.; Evdokiou, A.; Losic, D.; Santos, A. Facile Synthesis of Optical Microcavities by a Rationally Designed Anodization Approach: Tailoring Photonic Signals by Nanopore Structure. *ACS Appl. Mater. Interfaces* **2015**, *7*, 9879-9888.

48. Law, C. S.; Lim, S. Y.; Abell, A. D.; Marsal, L. F.; Santos, A. Structural Tailoring of Nanoporous Anodic Alumina Optical Microcavities for Enhanced Resonant Recirculation of Light. *Nanoscale* **2018**, *10*, 14139-14152.

49. Chen, Y.; Santos, A.; Wang, Y.; Kumeria, T.; Ho, D.; Li, J.; Wang, C.; Losic, D. Rational Design of Photonic Dust from Nanoporous Anodic Alumina Films: A Versatile Photonic Nanotool for Visual Sensing. *Sci. Rep.* **2015**, *5*, 12893.

50. Sukarno; Law, C. S.; Santos, A. Realisation and Optical Engineering of Linear Variable Bandpass Filters in Nanoporous Anodic Alumina Photonic Crystals. *Nanoscale* **2017**, *9*, 7541-7550.

51. Santos, A.; Yoo, J. H.; Rohatgi, C. V.; Kumeria, T.; Wang, Y.; Losic, D. Realisation an Advanced Engineering of True Optical Rugate Filters Based on Nanoporous Anodic Alumina by Sinusoidal Pulse Anodisation. *Nanoscale* **2016**, *8*, 1360-1373.

52. Lim, S. Y.; Law, C. S.; Marsal, L. F.; Santos, A. Engineering of Hybrid Nanoporous Anodic Alumina Photonic Crystals by Heterogeneous Pulse Anodization. *Sci. Rep.* **2018**, *8*, 9455.

53. Abràmoff, M. D.; Magalhães, P. J.; Ram, S. J. Image Processing with ImageJ. *Biophotonics Inter.* **2004**, *11*, 36-42.

54. Nishimura, S.; Abrams, N.; Lewis, B. A.; Halaoui, L. I.; Malluok, T. E.; Benkstein, K.D.; van de Lagemaat, J.; Frank, A. J. Standing Wave Enhancement of Red Absorbance and Photocurrent in Dye-Sensitized Titanium Dioxide Photoelectrodes Coupled To Photonic Crystals. *J. Am. Chem. Soc.* **2003**, *125*, 6306-6310.

55. Li, Y.; Kunitake, T.; Fujikawa, S. Efficient Fabrication and Enhanced Photocatalytic Activities of 3D-Ordered Films of Titania Hollow Spheres. *J. Phys. Chem. B* **2006**, *110*, 13000-13004.

56. Deparis, O.; Mouchet, S. R.; Su, B.-L. Light Harvesting in Photonic Crystals Revisited: Why do Slow Photons at the Blue Edge Enhance Absorption? *Phys. Chem. Chem. Phys.* **2015**, *17*, 30525-30532.

57. Brzózka, A.; Brudzisz, A.; Hnida, K.; Sulka, G. D. Chemical and Structural Modifications of Nanoporous Alumina and Its Optical Properties. In *Electrochemically Engineered Nanoporous Materials: Methods, Properties and Applications*; Losic, D., Santos, A., Eds.; Springer International Publishing: Cham, 2015; Vol. 220, pp. 219-288.

58. Kim, S.; Choi, W. Visible-Light-Induced Photocatalytic Degradation of 4-Chlorophenol and Phenolic Compounds in Aqueous Suspension of Pure Titania: Demonstrating the Existence of a Surface-Complex-Mediated Path. *J. Phys. Chem. B* **2005**, *109*, 5143-5149.

59. Lee, K.; Mazare, A.; Schmuki, P. One-Dimensional Titanium Dioxide Nanomaterials: Nanotubes. *Chem. Rev.* **2014**, *114*, 9385-9454.

60. Lettmann, C.; Hildenbrand, K.; Kisch, H.; Macyk, W.; Maier, W.F. Visible Light Photodegradation of 4-Chlorophenol with a Coke-Containing Titanium Dioxide Photocatalyst. *Appl. Catal. B* **2001**, *32*, 215-227.

TABLE OF CONTENTS